

Adaptive Decoding Mechanisms for UAV-enabled Double-Uplink Coordinated NOMA

Thanh Luan Nguyen, Georges Kaddoum, *Senior Member, IEEE*, Tri Nhu Do, Daniel Benevides da Costa, *Senior Member, IEEE* and Zygmunt J. Haas, *Fellow, IEEE*

Abstract—In this paper, we propose a novel adaptive decoding mechanism (ADM) for the unmanned aerial vehicle (UAV)-enabled uplink (UL) non-orthogonal multiple access (NOMA) communications. Specifically, considering a harsh UAV environment where ground-to-ground links are regularly unavailable, the proposed ADM overcomes the challenging problem of conventional UL-NOMA systems whose performance is sensitive to the transmitter’s statistical channel state information and the receiver’s decoding order. To evaluate the performance of the ADM, we derive closed-form expressions for the system outage probability (OP) and throughput. In the performance analysis, we provide novel expressions for practical air-to-ground and ground-to-air channels while taking into account the practical implementation of imperfect successive interference cancellation (SIC) in UL-NOMA. These results have not been previously reported in the technical literature. Moreover, the obtained expression can be adopted to characterize the OP of various systems under a Mixture of Gamma (MG) distribution-based fading channels. Next, we propose a sub-optimal Gradient Descent-based algorithm to obtain the power allocation coefficients that result in maximum throughput with respect to each location on UAV’s trajectory, which follows a random waypoint mobility model for UAVs. Numerical solutions show that the ADM significantly improves the performance of UAV-enabled UL-NOMA, particularly in mobile environments.

Index Terms—NOMA, UAV, uplink, adaptive decoding, outage probability, throughput, mobility model, optimization.

I. INTRODUCTION

Due to its potential for wide-area coverage, scalability, service continuity, and improved availability [1], the development of non-terrestrial networks (NTNs) is attracting significant research interests, fueled by the introduction of the beyond-fifth-generation (B5G) and the sixth generation (6G) wireless networks. NTNs include low-altitude platforms (LAPs), which have been proposed for various military and civilian mission critical applications [2]. Among key components of LAPs are unmanned aerial vehicles (UAVs), which are flexible, low cost, and close to the ground platforms. As a result, a variety of

UAV-based applications have been proposed, including physical layer security and emergency communications in post-disaster scenarios or in unexpected events [3]. UAVs can also act as aerial relays in cooperative wireless communications to assist users with poor channel conditions, such as in cell-edge locations in cellular networks [4]. The reason for this is that UAVs can change their position to improve channel conditions, allowing the performance of cooperative transmissions to be greatly improved even when direct communication between the transmitter and the receiver is unavailable.

In addition to NTN, future B5G and 6G wireless networks will require efficient multiple access (MA) techniques to effectively exploit available resources such as frequency, time, power, and code, and to ensure multiple users meet their quality-of-service (QoS) requirements. In light of such concerns, non-orthogonal multiple access (NOMA) was shown to be a promising technique and has attracted considerable attention from both academia and industry [5]–[7]. In NOMA, the receivers recover information received from paired transmitters, by employing successive interference cancellation (SIC) with a designed decoding order [8], [9]. As a result, the use of NOMA provides additional degrees of freedom in the power domain and enhancement of spectrum utilization. This promising technique has been intensively investigated in the literature in various systems, such as coordinated direct and relay transmission (CDRT-NOMA) [10], [11], massive multiple-input-multiple-output (mMIMO-NOMA) [12], secure systems [13], and reconfigurable intelligent surface networks (IRS-NOMA) [14].

However, in the aforementioned studies, limited efforts have been made to integrate UAVs with CDRT-NOMA to improve the performance of cell-edge users in wireless cellular networks. The use of UAVs in CDRT-NOMA systems can increase the coverage area of the underlying system, extend the communication range of cell-edge users, and provide higher spectral efficiency. In particular, in CDRT-NOMA, a central node, such as a base station or fusion center, communicates with nearby nodes over direct links, while cell-edge users that cannot use direct links are assisted by intermediate relays using cooperative communication. In the literature, there has been several works addressing downlink CDRT-NOMA [10], [15]. In [10], the authors presented an CDRT-NOMA scheme for IoT networks seeking to improve the spectrum efficiency (SE). The authors provided results for the outage probability (OP) and Ergodic Sum Capacity (ESC). The study in [15] proposed spectrum-efficient schemes for CDRT-NOMA under the assumption of Nakagami- m fading channels. However,

T.-L. Nguyen, G. Kaddoum and T. N. Do are with the Department of Electrical Engineering, the École de Technologie Supérieure (ÉTS), Université du Québec, Montréal, QC H3C 1K3, Canada (emails: thanh-luan.nguyen.1@ens.etsmtl.ca, georges.kaddoum@etsmtl.ca, tri-nhu.do@etsmtl.ca).

D. B. da Costa is with the AI & Telecom Research Center, Technology Innovation Institute, 9639 Masdar City, Abu Dhabi, United Arab Emirates (email: danielbcosta@ieee.org).

Z. J. Haas is with the Department of Computer Science, University of Texas at Dallas, Richardson, TX 75080, USA, and also with the School of Electrical and Computer Engineering, Cornell University, Ithaca, NY 14853, USA (e-mail: zhaas@cornell.edu).

studies on uplink (UL) scenarios are quite limited, which can prevent CDRT-NOMA systems from being deployed in a variety of applications such as navigation, disaster relief, and ubiquitous data collection.

In conventional UL CDRT-NOMA, there are two information transmission phases [11], [16]–[18]. The first phase involves the cell-center user (UE-C) and the cell-edge user (UE-E) transmitting information to a fusion center (FC) and an intermediate relay, respectively. In this context, the UE-E does not affect the information reception at the FC; however, the UE-C causes interference at the relay. In the second phase, the UE-C transmits new information, and the relay node forwards the decoded information from UE-E, causing interference at the FC. In both phases, by exploiting the distinct channel gain of the transmitters, the SIC receivers at the relay and at the FC can correctly decode the desired information signals. The study in [19] proposed an UL CDRT-NOMA scheme and derived the ESC under both perfect and imperfect SIC at the receivers, showing a significant capacity improvement compared to traditional orthogonal multiple access (OMA) schemes. In [11], the authors proposed relaying schemes that improve the system throughput of two-user CDRT-NOMA and designed network-coded strategies to improve the system throughput when the transmitters have similar channel conditions. Moreover, the authors in [17] considered hybrid device-to-device (D2D) and uplink CDRT-NOMA to enhance the SE and extend the coverage area of the cellular network. Considering downlink CDRT-NOMA, the research in [18] proposed a joint downlink and uplink schemes for bidirectional communication, which can improve the ESR, and the receive reliability of edge users.

In the aforementioned works, the use of UAVs as intermediate relays has not been discussed. Existing UL CDRT-NOMA schemes cannot simply treat terrestrial relays as UAVs as there exist some challenges. In these schemes, the non-adaptive SIC order is based on the statistical channel state information (CSI) of the transmitters, where the receiver exploits a large amount of instantaneous CSI to decode the received signals from the transmitters [20]–[22]. In [20], based on statistical CSI, the authors derived the OP of multi-user UL NOMA schemes over Rayleigh channels. An extension to generalized fading was developed in [21]. A recent research on use of CDRT-NOMA in Internet-of-Things (IoT) networks promoting statistical CSI-based decoding order was reported in [22]. However, due to the high mobility of UAVs, the statistical CSI of the UAV to terrestrial device links fluctuates dynamically as the UAV travels in the three-dimensional (3D) space [23], [24]. As a result, the UAV and FC can experience extreme interference due to the non-adaptive decoding orders, leading to incorrect signal segregation at the SIC receivers, which limits the application of such schemes. To address this issue, a more adaptive SIC ordering should be considered.

The available decoding mechanisms in [25]–[27] require not only perfect channel state information (CSI), but also information about the power control strategy. The studies in [25], [26], in particular, present dynamic decoding orders for uplink NOMA transmission, where dynamic SIC receivers estimate the received power from each transmitter before decoding the received signal. In addition, [27] proposed resource allocation

and power control algorithms for dynamic SIC receivers.

In this paper, we consider uplink CDRT-NOMA in wireless cellular networks, consisting a cell-center user (UE-C) with direct access to the fusion center (FC), and UE-E with no direct access to the FC. The UE-E requires a relay node, i.e., the UAV, to assist its communication to the FC. In contrast to related works, we consider an adaptive UL CDRT-NOMA transmission, where the UAV and the FC adaptively decode the UL signals by exploiting the UL channel power gains. The contributions of this paper can be summarized as follows:

- We propose novel adaptive decoding mechanisms (ADM) tailored for double-UL (D-UL) power-domain NOMA (PD-NOMA) systems. First, a PD-NOMA technique is introduced for D-UL transmissions from both UE-C and UE-E, which are different types of user equipments (UEs), to a FC with the assistance of an intermediate UAV. Then, to deal with the dynamic disparity in the UL channels, which can drastically reduces the performance of SIC-inherited systems, we propose novel ADM performed at the UAV and the FC.
- Under this setting, a new framework is developed to derive the OP of the proposed system. It is noted that considering such complicated ADM-based D-UL results in several challenging OP formulas. To deal with these challenges, we first determine the outage events using unions and complements of stochastic events. Then, to formulate the overall system outage event, total probability and conditional probability theorems are taken into consideration. Finally, with the formulated overall system outage event, we drive closed-expressions for the OP with respect to each users and the overall system OP.
- To improve the cell-edge performance, we formulate an optimal power allocation strategy that minimizes the OP of the edge user. To this end, a fast-convergent Gradient Decent algorithm is proposed to achieve a near-optimal solution with a negligible optimality gap ¹.

Notations: $\mathbb{E}[\cdot]$ denotes expectation operator; $F_X(x)$ and $f_X(x)$ represent the cumulative distribution function (CDF) and probability density function (PDF) of an arbitrary random variable X , respectively; $\Pr[A]$ stands for the probability that an event A occurs; $\mathcal{CN}(0, \sigma^2)$ denotes a circular symmetric complex Gaussian random variable with zero-mean and variance σ^2 ; and $\Gamma(\cdot, \cdot)$ and $\gamma(\cdot, \cdot)$ denote the upper and lower incomplete gamma functions [28, Eq. (8.350.1)], respectively.

II. SYSTEM MODEL

Let us consider D-UL transmissions of an IoT system consisting an UE-C node and an UE-E node, communicating with a FC node, which can be wireless access point, as depicted in Fig. 1. Hereafter, let us use C, E, F and U as acronyms to represent UE-C, UE-E, FC, and UAV, respectively. Due to radio propagation impairments, the link between E and F is unavailable, thus the UL transmission of E relies on the assistance of an intermediate U, acting as a relay. Herein, U is considered to be hovering at a fixed altitude Z_U , and within

¹It is noted that our results are reproducible using our Matlab code, which is available at <https://github.com/thanhluannguyen/UAV-NOMA-ADM>.

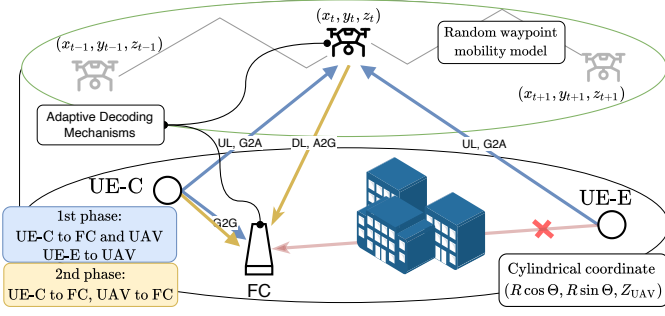


Fig. 1. The proposed UAV-aided D-UL coordinated NOMA with ADM.

a circle with the radius R and the center is F . We adopt the three-dimensional (3D) Cartesian coordinates system to model the locations of C , E , F , and U as (X_C, Y_C, Z_C) , (X_E, Y_E, Z_E) , (X_F, Y_F, Z_F) and (X_U, Y_U, Z_U) , respectively. The equivalent coordinates of U in the 3D cylindrical coordinates system are given as $(R \cos \Theta, R \sin \Theta, Z_U)$, where R and Θ are the radius and angular coordinates of U , respectively. The distance between X and Y , denoted as d_{XY} , can be formulated as

$$d_{XY} = \sqrt{(X_Y - X_X)^2 + (Y_Y - Y_X)^2 + (Z_Y - Z_X)^2}, \quad (1)$$

where $XY \in \{CU, UF, CF, EU\}$.

Let us denote h_{XY} as the channel coefficient between the nodes X and Y , and assume that all channels are reciprocal. The channel coefficient h_{XY} can be expressed as

$$h_{XY} = g_{XY} e^{j\angle h_{XY}} \sqrt{\mathcal{L}_{XY}}, \quad (2)$$

where g_{XY} and $\angle h_{XY}$ are the magnitude and phase of the small-scale fading, respectively, and $\sqrt{\mathcal{L}_{XY}}$ is the large-scale fading. In addition, the D-UL transmission scheme can be divided into two phases as follows. During the first phase, of duration t_1 , C and E transmit their information; i.e., $x_C^{[1]}$ and x_E , to F and U , respectively. During the second phase of duration t_2 , C and U convey $x_C^{[2]}$ and \hat{x}_E to F , respectively.

A. Ground-to-Ground (G2G) Channel Model

We assume that C is located in a dense urban area (DUA) and within some distance of F . In other words, the line-of-sight (LoS) links between C and F can be impacted by shadowing, such as being obscured by buildings. In this paper, we assume the channel between C and F follows the shadowed Rician fading model, where the probability density function (PDF) of g_{CF}^2 is given by [29]

$$f_{g_{CF}^2}(x) = \alpha \sum_{l=1}^{m_{CF}-1} \zeta(l) \frac{x^l}{l!} e^{-(\beta-\delta)x} + \alpha e^{-(\beta-\delta)x}, \quad x > 0, \quad (3)$$

where $\zeta(l) \triangleq \frac{(-1)^l (1-m_{CF})_l \delta^l}{l!}$ with $(\cdot)_l$ being the Pochhammer symbol [30], m_{CF} is the shadowing severity parameter, $\beta \triangleq \frac{1}{2b}$, $\alpha \triangleq \frac{1}{2b} \left(\frac{2bm_{CF}}{2bm_{CF} + \Omega_{CF}} \right)^{m_{CF}}$, and $\delta \triangleq \frac{\Omega_{CF}}{2b(2bm_{CF} + \Omega_{CF})}$ with Ω_{CF} and $2b$ being the average power of the LoS and multipath components, respectively.

For the large-scale fading, we consider the 3GPP Urban Micro (UMi) path loss model for LoS communication, where the path loss \mathcal{L}_{XY} is given by [31, Table B.1.2.1-1]

$$\mathcal{L}_{CF} [\text{dB}] = G_C [\text{dB}] + G_F [\text{dB}] - 22.7 - 26 \log(f_c) - 36.7 \log(d_{CF}/d_0), \quad (4)$$

where G_C and G_F are the transmit and receive antenna gains at C and F , respectively, f_c is the carrier frequency, and $d_0 = 1$ [m] is the reference distance.

B. Air-to-Ground (A2G) and Ground-to-Air (G2A) Channel Models

In our model, there may be limited information on the precise locations, heights, and amount of radio impairments, such as due to buildings, walls, and so on. Meanwhile, the randomness associated with the LoS and non-line-of-sight (NLoS) links must be considered in the design of the UAV-based communication system. As a result, to develop practical A2G/G2A channels, we consider that each device, i.e., E , C , and F , has a probabilistic LoS link towards U . The LoS probability is a function of the device's and U 's locations in the 3D plane. One popular approach for determining the LoS probability in DUAs is based on a logistic function, which is expressed as [32]

$$p_{XY}^{\text{LoS}} = \frac{1}{1 + 12.08 \exp(-0.11(J_{XY} - 12.08))}, \quad (5)$$

where J_{XY} , measured in degrees, denotes the elevation angle. Specifically, J_{XY} can be calculated as

$$J_{XY} = \frac{180}{\pi} \arcsin \frac{|Z_Y - Z_X|}{d_{XY}}, \quad (6)$$

where $|\cdot|$ denotes the absolute value operator. Accordingly, the probability of having a NLoS connection is the complementary of (5); i.e., $p_{XY}^{\text{NLoS}} = 1 - p_{XY}^{\text{LoS}}$. The PDF of the magnitude g_{XY} for the A2G/G2G channels can be modelled as [33]

$$f_{g_{XY}}(x; m) = \begin{cases} \frac{2m^m}{(m-1)!} x^{2m-1} e^{-mx^2}, & \text{for LoS link,} \\ 2xe^{-x^2}, & \text{for NLoS link,} \end{cases} \quad (7)$$

for $x > 0$, where m is the shape factor, which corresponds to the Nakagami- m fading for LoS link.

The path loss of the A2G/GA2 channels in a DUA takes into account both probabilistic LoS and NLoS conditions, where the path loss for LoS and NLoS paths are modeled as [33]

$$\mathcal{L}_{XY} [\text{dB}] = 20 \log_{10} \left(\frac{c}{4\pi d_{XY} f_c} \right) - \begin{cases} \eta [\text{dB}], & \text{for LoS link,} \\ \bar{\eta} [\text{dB}], & \text{for NLoS link,} \end{cases} \quad (8)$$

where c is the speed of light, η and $\bar{\eta}$ are the link attenuation under LoS and NLoS conditions, respectively.

C. The Proposed ADM

Note that with the proposed D-UL transmission, the performance of C is not compromised by time-division in DF relaying as is used in conventional relaying schemes, and the severe fading conditions experienced by E can be remedied, guaranteeing a reliable communication. Such an application of this scheme is employed when the delay-limited service-based UE-C requires high data rate (e.g. video streaming services), whereas the delay-tolerant service-based UE-E demands a reliable communication.

D. The First UL Phase

Following the settings of PD-NOMA-aided uplink transmission [34] during the first phase, E and C simultaneously transmit x_E and $x_C^{[1]}$ to U and F, respectively. The transmission powers of E and C are denoted by $P_C^{[1]}$ and P_E , respectively, where $P_C^{[1]} + P_E \leq P_{\max}^{[1]}$ with $P_{\max}^{[1]}$ being the maximum power budget in the first phase. Hence, the received signals at U and F are, respectively, formulated as

$$y_U^{[1]} = h_{CU}x_C^{[1]} + h_{EU}x_E + n_U^{[1]}, \quad (9)$$

$$y_F^{[1]} = h_{CF}x_C^{[1]} + n_F^{[1]}, \quad (10)$$

where $\mathbb{E} \left[|x_C^{[1]}|^2 \right] = P_C^{[1]}$, $\mathbb{E} \left[|x_E|^2 \right] = P_E$, $n_U^{[1]} \sim \mathcal{CN}(0, \sigma_U^2)$, and $n_F^{[1]} \sim \mathcal{CN}(0, \sigma_F^2)$ are the zero means additive white Gaussian noises (AWGNs) at U and F, respectively, with σ_U^2 and σ_F^2 being the corresponding noise powers.

From (10), F decodes $x_C^{[1]}$ with the achievable rate

$$R_{F, x_C^{[1]}} = \frac{t_1}{T} \log_2 \left(1 + \frac{P_C^{[1]} |h_{CF}|^2}{\sigma_F^2} \right) \quad (11)$$

$$= \frac{t_1}{T} \log_2 \left(1 + \frac{P_C^{[1]} g_{CF}^2 \mathcal{L}_{CF}}{\sigma_F^2} \underbrace{e^{\mathcal{L}_{CF}}}_{=1} \right). \quad (12)$$

Meanwhile, by exploiting the disparity in the gains $g_{CU}^2 \mathcal{L}_{CU}$ and $g_{EU}^2 \mathcal{L}_{EU}$, U determines an effective decoding mechanism to guarantee reliable transmission at E. Specifically, the proposed ADM at U are described as follows.

In the scenario that $\mathbb{E}_{C \rightarrow E} \triangleq [g_{CU}^2 \mathcal{L}_{CU} \geq g_{EU}^2 \mathcal{L}_{EU}]$, the channel from U to C is stronger than from U to E, U decodes $x_C^{[1]}$ and cancels it from $y_U^{[1]}$ using SIC. Then, the desired signal for U, x_E , is decoded. From (9), U decodes $x_C^{[1]}$ with the achievable rate given by

$$R_{U, x_C^{[1]} | \mathbb{E}_{C \rightarrow E}^{[U]}} = \frac{t_1}{T} \log_2 \left(1 + \frac{P_C(t_1) g_{CU}^2 \mathcal{L}_{CU}}{P_E g_{EU}^2 \mathcal{L}_{EU} + \sigma_U^2} \right). \quad (13)$$

In practice, U cannot perfectly cancel $x_C^{[1]}$ from $y_U^{[1]}$ with SIC, which incurs an amount of residual power from $x_C^{[1]}$ and causes additional interference while U decodes x_E . Subsequently, U decodes x_E with the instantaneous achievable rate given by

$$R_{U, x_E | \mathbb{E}_{C \rightarrow E}^{[U]}} = \frac{t_1}{T} \log_2 \left(1 + \frac{P_E g_{EU}^2 \mathcal{L}_{EU}}{P_C^{[1]} |\tilde{h}_{CU}|^2 + \sigma_U^2} \right), \quad (14)$$

where the $P_C^{[1]} |\tilde{h}_{CU}|^2$ specifies the interference power from imperfectly removing $x_C^{[1]}$, \tilde{h}_{CU} can be modeled as $\tilde{h}_{CU} \sim \mathcal{CN}(0, \xi_U \mathbb{E} [|h_{CU}|^2])$ with $0 \leq \xi_U \leq 1$ being the residual interference (RI) level [16]. It is noteworthy that \tilde{h}_{CU} and h_{CU} are independent random variables (RVs) and $\xi_U = 0$ represents perfect SIC.

In the scenario $\mathbb{E}_{E \rightarrow C}^{[U]} \triangleq [g_{CU}^2 \mathcal{L}_{CU} < g_{EU}^2 \mathcal{L}_{EU}]$, which is the complementary of $\mathbb{E}_{C \rightarrow E}^{[U]}$, U attempts to decode x_E while treating $x_C^{[1]}$ as interference. Since the main objective of cooperative communication is to forward E's information signal to F, we only consider the decoding of x_E and neglect $x_C^{[1]}$. Subsequently, U decodes x_E with the achievable rate given by

$$R_{U, x_E | \mathbb{E}_{E \rightarrow C}^{[U]}} = \frac{t_1}{T} \log_2 \left(1 + \frac{P_E g_{EU}^2 \mathcal{L}_{EU}}{P_C^{[1]} g_{CU}^2 \mathcal{L}_{CU} + \sigma_U^2} \right). \quad (15)$$

Recalling that the sole purpose of deploying an additional UAV is to assist E, thus a seemingly promising approach is to focus on decoding x_E and then forwards \hat{x}_E to F. As a result, U may experience critical outage when the channel from C to U is stronger than the channel from E to U. Under $\mathbb{E}_{C \rightarrow E}^{[U]}$, the ADM at U can avoid such an outage event by directly decoding $x_C^{[1]}$. Under $\mathbb{E}_{E \rightarrow C}^{[U]}$, the ADM at U considers that E-U link is stronger than C-U link, which results in the direct decoding of \hat{x}_E without wasting power on performing SIC.

E. The Second Uplink Phase

Assuming U correctly decodes x_E in the first phase, it forwards \hat{x}_E in the second phase. Meanwhile, C also transmits $x_C^{[2]}$, which is different from $x_C^{[1]}$. In addition, assuming that the transmission powers of C and U in the second phase are $P_C^{[2]}$ and P_U , respectively, where $P_C^{[2]} + P_U \leq P_{\max}^{[2]}$ with $P_{\max}^{[2]}$ being the maximum power budget during this phase, the received signal at F in the case that x_E is correctly decoded is expressed as

$$y_F^{[2]} = h_{UF} \hat{x}_E + h_{CF} x_C^{[2]} + n_F^{[2]}. \quad (16)$$

Similarly, we also consider ADM at F, which are described as follows.

In the scenario that $\mathbb{E}_{C \rightarrow U}^{[F]} \triangleq [g_{CF}^2 \mathcal{L}_{CF} \geq g_{UF}^2 \mathcal{L}_{UF}]$, the channel from F to C is stronger than from F to U, F primarily decodes $x_C^{[2]}$ while treating \hat{x}_E as interference. In this case, F decodes $x_C^{[2]}$ with the achievable rate given by

$$R_{F, x_C^{[2]} | \mathbb{E}_{C \rightarrow U}^{[F]}} = \frac{t_2}{T} \log_2 \left(1 + \frac{P_C^{[2]} g_{CF}^2 \mathcal{L}_{CF}}{P_U g_{UF}^2 \mathcal{L}_{UF} + \sigma_F^2} \right). \quad (17)$$

Once $x_C^{[2]}$ is correctly decoded, F performs SIC in an attempt to remove $x_C^{[2]}$ from $y_F^{[2]}$ before decoding \hat{x}_E . Assuming imperfect SIC, F decodes \hat{x}_E with the achievable rate given by

$$R_{F, \hat{x}_E | \mathbb{E}_{C \rightarrow U}^{[F]}} = \frac{t_2}{T} \log_2 \left(1 + \frac{P_U g_{UF}^2 \mathcal{L}_{UF}}{P_C^{[2]} |\tilde{h}_{CF}|^2 + \sigma_F^2} \right), \quad (18)$$

where $P_C^{[2]} |\tilde{h}_{CF}|^2$ denotes the RI power due to the imperfect cancellation of $x_C^{[2]}$ at F, and $\tilde{h}_{CF} \sim \mathcal{CN}(0, \xi_F \mathbb{E}[|h_{CF}|^2])$ with $0 \leq \xi_F \leq 1$ being the RI level [16].

In the scenario $\mathbb{E}_{U \rightarrow C}^{[F]} \triangleq [g_{CF}^2 \mathcal{L}_{CF} < g_{UF}^2 \mathcal{L}_{UF}]$, which is the complementary of $\mathbb{E}_{C \rightarrow U}^{[F]}$, F primarily decodes \hat{x}_E while treating $x_C^{[2]}$ as interference. In this case, F decodes \hat{x}_E with the achievable rate given by

$$R_{F, \hat{x}_E | \mathbb{E}_{U \rightarrow C}^{[F]}} = \frac{t_2}{T} \log_2 \left(1 + \frac{P_U g_{UF}^2 \mathcal{L}_{UF}}{P_C^{[2]} g_{CF}^2 \mathcal{L}_{CF} + \sigma_F^2} \right), \quad (19)$$

Once \hat{x}_E is correctly decoded, F then performs SIC in an attempt to remove \hat{x}_E from $y_F^{[2]}$, then decodes $x_C^{[2]}$. Assuming imperfect SIC, F decodes $x_C^{[2]}$ with the achievable rate given by

$$R_{F, x_C^{[2]} | \mathbb{E}_{U \rightarrow C}^{[F]}} = \frac{t_2}{T} \log_2 \left(1 + \frac{P_C^{[2]} g_{CF}^2 \mathcal{L}_{CF}}{P_U |\tilde{h}_{UF}|^2 + \sigma_F^2} \right), \quad (20)$$

where $P_U |\tilde{h}_{UF}|^2$ denotes the residual power due to the imperfect cancellation of \hat{x}_E , and $\tilde{h}_{UF} \sim \mathcal{CN}(0, \xi_F \mathcal{L}_{CF})$.

While U is only required to correctly decode x_E , F is required to correctly decode both of the information signals of C and E. Not only so, F needs to maintain the fairness in the performance between \hat{x}_E and $x_C^{[2]}$. Under $\mathbb{E}_{C \rightarrow U}^{[F]}$, $x_C^{[2]}$ is transmitted over a dominant uplink, and thus should be decoded first to avoid interference while decoding \hat{x}_E . In addition, under $\mathbb{E}_{U \rightarrow C}^{[F]}$, F primarily decodes \hat{x}_E to meet E's quality-of-service (QoS) which in turn avoids extreme interference while F decodes $x_C^{[2]}$.

In addition, when U incorrectly decodes x_E , U remains silent during the second phase to avoid unnecessary interference to F. In this case, F only receives $x_C^{[2]}$ from C. As a result, the instantaneous rate at F is given by

$$R_{F, x_C^{[2]}} = \frac{t_2}{T} \log_2 \left(1 + \frac{P_C^{[2]} g_{CF}^2 \mathcal{L}_{CF}}{\sigma_F^2} \right). \quad (21)$$

It is noted that the proposed ADM at U aims to improve E's performance due to the fact that the direct link from E to F is not available. However, ADM at U can interfere with the decoding of $x_C^{[2]}$ at F during the second phase. To compensate for such performance loss, F adopts the proposed ADM to adaptively decode $x_C^{[2]}$ by exploiting the uplink channel conditions. Specifically, if U-F link is stronger than the C-F link, F avoids treating \hat{x}_E as interference and directly decodes $x_C^{[2]}$, which in turns avoids the dominant interference power from U. The proposed ADM algorithm is summarized as Algorithm 1.

III. PERFORMANCE ANALYSIS

A. Preliminaries

1) *G2G and A2G/G2A Channels Characterization*: In this subsection, we determine the statistical property of the G2G and A2G/G2A channel power gains. Let us denote $\phi_{XY} =$

Algorithm 1: Proposed ADM for UAV-aided D-UL CDRT-NOMA.

```

1 initialize: Received signals at U,  $y_U^{[1]}$ , and F,  $y_F(t_1)$ , in
   the phase  $t_1$ , isUAVSilent  $\leftarrow$  false,
   signalOut  $\leftarrow$  empty
2 if  $S_C^{[1]} : (12) > R_{th,C}$  then
3   | add  $x_C^{[1]}$  into signalOut.
4 else
5   | F fails to decode  $x_C^{[1]}$ .
6 if  $\mathbb{E}_{C \rightarrow E}^{[U]}$  occurs then
7   | if  $S_{C \rightarrow E}^{[U]} : (13) > R_{th,C}$  then
8     | U cancels  $x_C^{[1]}$  with imperfect SIC.
9     | if  $S_E^{[U]} : (14) > R_{th,E}$  then
10    | | isUAVSilent  $\leftarrow$  false
11    | | else
12    | | | isUAVSilent  $\leftarrow$  true.
13    | | else
14    | | | isUAVSilent  $\leftarrow$  true.
15 else if  $\mathbb{E}_{E \rightarrow C}^{[U]} : |h_{CU}|^2 < |h_{EU}|^2$  then
16   | if  $S_{E \rightarrow C}^{[U]} : (15) > R_{th,E}$  then
17     | | isUAVSilent  $\leftarrow$  false
18     | | else
19     | | | isUAVSilent  $\leftarrow$  true.
20 if not isUAVSilent then
21   | if  $\mathbb{E}_{C \rightarrow U}^{[F]} : |h_{CF}|^2 > |h_{UF}|^2$  then
22     | if  $S_{C \rightarrow U}^{[F]} : (17) > R_{th,C}$  then
23       | | add  $x_C^{[2]}$  into signalOut.
24       | | F cancels  $x_C^{[2]}$  with imperfect SIC. if
25         | | |  $S_U^{[F]} : (18) > R_{th,E}$  then
26           | | | | add  $\hat{x}_E$  into signalOut.
27         | | | else
28         | | | | F fails to decode  $\hat{x}_E$ .
29       | | else
30       | | | F fails to decode  $x_C^{[2]}$  and  $\hat{x}_E$ .
31   | else if  $\mathbb{E}_{U \rightarrow C}^{[F]}$  occurs then
32     | if  $S_{U \rightarrow C}^{[F]} : (19) > R_{th,E}$  then
33       | | add  $\hat{x}_E$  into signalOut.
34       | | F cancels  $\hat{x}_E$  with imperfect SIC.
35       | | if  $S_C^{[F]} : (20) > R_{th,C}$  then
36         | | | add  $x_C^{[2]}$  into signalOut.
37         | | | else
38         | | | | F fails to decode  $\hat{x}_E$ .
39       | | else
40       | | | F fails to decode  $x_C^{[2]}$  and  $\hat{x}_E$ .
41   | else
42     | if  $S_C^{[2]} : (21) > R_{th,C}$  then
43       | | add  $x_C^{[2]}$  into signalOut.
44     | | else
45       | | | F fails to decode  $x_C^{[2]}$  and  $\hat{x}_E$ .
46 output: signalOut.

```

$g_{XY}^2 \mathcal{L}_{XY}$ as the power gain of the X-Y link. For the G2G channel from C to F, the PDF of ϕ_{CF} is given by

$$f_{\phi_{XY}}(x) = \alpha \sum_{l=1}^{m_{CF}-1} \zeta(l) \frac{x^l}{l!} e^{-\frac{\beta-\delta}{\zeta_{CF}} x} + \alpha e^{-\frac{\beta-\delta}{\zeta_{CF}} x}. \quad (22)$$

In addition, the PDF of the A2G/G2A channel gains can be expressed as

$$f_{\phi_{XY}}(x) = p_{XY} \frac{\left(\frac{\eta}{m} \left(\frac{4\pi d_{XY}}{c/f_c} \right)^2 \right)^{-m_{XY}}}{(m_{XY}-1)!} x^{m_{XY}-1} e^{-\frac{x}{\frac{\eta}{m} \left(\frac{4\pi d_{XY}}{c/f_c} \right)^2}} + \frac{1-p_{XY}}{\bar{\eta} \left(\frac{4\pi d_{XY}}{c/f_c} \right)^2} e^{-\frac{x}{\bar{\eta} \left(\frac{4\pi d_{XY}}{c/f_c} \right)^2}}, x > 0. \quad (23)$$

Let us denote $\varphi_{XY} \triangleq |\tilde{h}_{XY}|^2$ as the fraction of RI power due to imperfect SIC; thus, the PDF of φ_{XY} can be expressed as $f_{\varphi_{XY}}(x) = \frac{\bar{\zeta}_{XY}^{-1}}{\xi_Y} e^{-x \frac{\bar{\zeta}_{XY}^{-1}}{\xi_Y}}$, $x > 0$, where $\bar{\zeta}_{CF} = \mathcal{L}_{CF}$, and

$$\bar{\mathcal{L}}_{XY} = p_{XY} \frac{\left(\frac{c}{f_c} \right)^2}{4\pi d_{XY}} + (1-p_{XY}) \frac{\left(\frac{c}{f_c} \right)^2}{\bar{\eta}}. \quad (24)$$

By combining (22) and (23) into one unified expression, we then obtain the following Lemma.

Lemma 1. *The PDF and cumulative distribution function (CDF) of a $K_n + 1$ Mixture of Gamma (MG) distributions [35], each with shape $\mu_n(k)$ and scale $\Omega_n(k)$, are expressed as*

$$f_{\hat{\gamma}_n}(K_n, \hat{\Theta}_n; x) = \sum_{k=1}^{K_n+1} \chi_n(k) \frac{\Omega_n(k)^{-\mu_n(k)}}{(\mu_n(k)-1)!} x^{\mu_n(k)-1} e^{-\frac{x}{\Omega_n(k)}}, \quad (25)$$

$$F_{\hat{\gamma}_n}(K_n, \hat{\Theta}_n; x) = 1 - \sum_{k=1}^{K_n+1} \frac{\chi_n(k)}{(\mu_n(k)-1)!} \Gamma\left(\mu_n(k), \frac{x}{\Omega_n(k)}\right), \quad (26)$$

respectively, where $\Gamma(a, x)$ is the upper incomplete Gamma function [28], $\hat{\Theta}_n \triangleq [\hat{\theta}_n(1), \dots, \hat{\theta}_n(K_n + 1)]^T$ contains parameters of the MG distribution, and $\hat{\theta}_n(k) \triangleq (\chi_n(k), \Omega_n(k), \mu_n(k))$ denotes the vector containing parameters of the k -th Gamma distribution in the summation.

By adopting Lemma 1, we can remodel the G2G, A2G/G2A channel power gains, ϕ_{XY} , and the portion of RI power, φ_{XY} , as MG variates in the following Corollaries. It is worth noting that the results in the following sections can be adopted to characterize various systems over fading channels having MG-like distribution, e.g., $\kappa - \mu$ shadowed, Rician shadowed, generalized- K , and Rician [35].

Corollary 1. *The G2G channel power gain, ϕ_{CF} , can be modelled as a MG variate and denoted as $\hat{\gamma}_n \sim \phi_{CF}$, where*

$$\hat{\theta}_n(k) = \begin{cases} \left(\frac{\alpha \zeta(k)}{(\beta-\delta)^{k+1}}, \frac{\mathcal{L}_{XY}}{\beta-\delta}, k+1 \right), & 1 \leq k \leq K_n, \\ \left(\frac{\alpha}{\beta-\delta}, \frac{\mathcal{L}_{XY}}{\beta-\delta}, 1 \right), & \text{otherwise.} \end{cases} \quad (27)$$

Corollary 2. *The A2G/G2A channel power gains, ϕ_{XY} , for $XY \in \{\text{CU}, \text{UF}, \text{EU}\}$, can be modelled by a MG variate and denoted as $\hat{\gamma}_n \sim \phi_{XY}$, where*

$$\hat{\theta}_n(k) = \begin{cases} \left(p_{XY}, \frac{\left(\frac{c/f_c}{4\pi d_{XY}} \right)^2}{\eta m_{XY}}, m_{XY} \right), & 1 \leq k \leq K_n, \\ \left(1-p_{XY}, \frac{\left(\frac{c/f_c}{4\pi d_{XY}} \right)^2}{\bar{\eta}}, 1 \right), & \text{otherwise.} \end{cases} \quad (28)$$

Corollary 3. *The fraction of RI power, φ_{XY} , for $XY \in \{\text{CU}, \text{CF}, \text{UF}\}$, can be modelled by a MG variate and denoted as $\hat{\gamma}_n \sim \varphi_{XY}$, where*

$$\hat{\theta}_n(k) = \left(\frac{1}{2}, \xi_Y \bar{\mathcal{L}}_{XY}, 1 \right), \quad \forall k. \quad (29)$$

2) *Preliminary Integrals:* In this subsection, we introduce important integrals to assist with the forthcoming analysis. Without these integrals, our analysis would become extremely lengthy. Specifically, given that

$$\mathbf{w} \triangleq \mathbf{Q}\mathbf{x} + \mathbf{q}, \quad (30)$$

where $\mathbf{w} \triangleq (w_i) \in \mathbb{R}^{n \times 1}$, $\mathbf{Q} \triangleq \text{diag}(\mathbf{p}) \in \mathbb{R}^{n \times n}$, $\mathbf{p} \triangleq (p_i) \in \mathbb{R}^{n \times 1}$, $\mathbf{x} \triangleq (x_{i+1}) \in \mathbb{R}^{n \times 1}$, and $\mathbf{q} \triangleq (q_i) \in \mathbb{R}^{n \times 1}$, $0 \leq i \leq n$, the integrals are defined as

$$I_n = \int_D \left[\prod_{t=0}^n f_{\hat{\gamma}_t}(x_t) \right] d\mathbf{x}, \quad n = 1, 2, \dots \quad (31)$$

where $D \triangleq \{\mathbf{x} : [\mathbf{x}]_i \geq [\mathbf{w}]_i, 0 \leq i \leq n\}$ is the integration domain. It is noted that (31) represents the integral of the joint multiple MG-based distribution, which is $\prod_{t=0}^n f_{\hat{\gamma}_t}(x_t)$, over the integration domain D . Let $\hat{\gamma}_n$ be an RV whose PDF and CDF are $f_{\hat{\gamma}_n}(x)$ and $F_{\hat{\gamma}_n}(x)$, respectively, then the integral (31) can be derived from the following probabilities

$$I_n = \Pr \left[\bigcap_{t=0}^n \hat{\gamma}_t > [\mathbf{p}]_{t+1} \hat{\gamma}_{t+1} + [\mathbf{q}]_{t+1} \right] \quad (32)$$

$$= \Pr \left[\begin{bmatrix} \hat{\gamma}_0 \\ \hat{\gamma}_1 \\ \vdots \\ \hat{\gamma}_n \end{bmatrix} > \mathbf{Q} \begin{bmatrix} \hat{\gamma}_1 \\ \hat{\gamma}_2 \\ \vdots \\ \hat{\gamma}_{n+1} \end{bmatrix} + \mathbf{q} \right] \quad (33)$$

$$\triangleq \Pr [\hat{\gamma}_n > \mathbf{Q}\hat{\gamma}_{n+1} + \mathbf{q}], \quad (34)$$

where $\hat{\gamma}_i \triangleq [\hat{\gamma}_i, \hat{\gamma}_{i-1}, \dots, \hat{\gamma}_{i-n}]$.

For the exact closed-form expression (ECFE) of I_0 , we obtain $I_0 = \int_0^x f_{\hat{\gamma}_0}(x_0) dx_0 = F_{\hat{\gamma}_0}(x)$; thus,

$$I_0 = \sum_{k_0=1}^{K_0+1} \frac{\Xi_0(k_0)}{(\Lambda_0)^{-\kappa_0}} \Gamma\left(\kappa_0, \frac{w_0}{\Lambda_0}\right), \quad (35)$$

where $\Xi_0(k_0) \triangleq \frac{\chi_0(k_0)}{(\mu_0(k_0)-1)!} \Omega_0(k_0)^{-\mu_0(k_0)}$, $\Lambda_0 \triangleq \Omega_0(k_0)$, and $\kappa_0 \triangleq \mu_0(k_0)$. Accordingly, the ECFEs of I_1 and I_2 are derived in Lemma 2, and they are utilized to assist the analysis in the subsequent sections.

Lemma 2. The ECFEs of I_1 and I_2 are given by

$$I_1 = \sum_{k_0=1}^{K_0+1} \sum_{k_1=1}^{K_1+1} \sum_{i_0=0}^{\kappa_0-1} \sum_{j_0+l_0=i_0} \Xi_1(k_1) \frac{\Gamma\left(\kappa_1, \frac{w_1}{\Lambda_1}\right)}{(\Lambda_1)^{-\kappa_1}} \times \underbrace{\frac{\Xi_0(k_0)}{(\Lambda_0)^{i_0}} \frac{(q_0)^{j_0}}{j_0!} \frac{(p_0)^{l_0}}{l_0!} (\kappa_0 - 1)! \frac{e^{-\frac{q_0}{\Lambda_0}}}{(\Lambda_0)^{-\kappa_0}}}{\Phi_0(\mathbf{p}, \mathbf{q})}, \quad (36)$$

and

$$I_2 = \sum_{k_0=1}^{K_0+1} \sum_{k_1=1}^{K_1+1} \sum_{k_2=1}^{K_2+1} \sum_{i_0=0}^{\kappa_0-1} \times \sum_{j_0+l_0=i_0}^{\kappa_1-1} \sum_{i_1=0}^{\kappa_1-1} \sum_{j_1+l_1=i_1} \Xi_2(k_2) \frac{\Gamma\left(\kappa_2, \frac{w_2}{\Lambda_2}\right)}{(\Lambda_2)^{-\kappa_2}} \times \underbrace{\Phi_0(\mathbf{p}, \mathbf{q}) \frac{\Xi_1(k_1)}{(\Lambda_1)^{i_1}} \frac{(q_1)^{j_1}}{j_1!} \frac{(p_1)^{l_1}}{l_1!} (\kappa_1 - 1)! \frac{e^{-\frac{q_1}{\Lambda_1}}}{(\Lambda_1)^{-\kappa_1}}}{\Phi_1(\mathbf{p}, \mathbf{q})}, \quad (37)$$

where $\Lambda_n \triangleq \frac{1}{\frac{1}{\Omega_n(k_n)} + \frac{p_{n-1}}{\Lambda_{n-1}}}$, $\kappa_n \triangleq \mu_n(k_n) + l_{n-1}$, $\forall n \geq 1$, and $\Xi_n(k_n) \triangleq \frac{\chi_n(k_n)}{(\mu_n(k_n)-1)!} \Omega_n(k_n)^{-\mu_n(k_n)}$, $\forall n \geq 0$.

Proof: See Appendix A. ■

In general, the ECFE of I_n is given by

$$I_n = \sum_{K \geq k_n \geq 0} \sum_{\kappa \geq i \geq 0} \sum_{j+i=i} \Xi_n(k_n) \frac{\Gamma\left(\kappa_n, \frac{w_n}{\Lambda_n}\right)}{(\Lambda_n)^{-\kappa_n}} \Phi_{n-1}(\mathbf{p}, \mathbf{q}), \quad (38)$$

where $\sum_{K \geq k_n \geq 0} \equiv \sum_{k_0=1}^{K_0+1} \sum_{k_1=1}^{K_1+1} \dots \sum_{k_n=1}^{K_n+1}$, $\sum_{\kappa \geq i \geq 0} \equiv \sum_{j+i=i}^{\kappa_0-1} \sum_{j_0+l_0=i_0} \dots \sum_{i_{n-1}=0}^{\kappa_{n-1}-1} \sum_{j_{n-1}+l_{n-1}=i_{n-1}}$, and

$$\Phi_n(\mathbf{p}, \mathbf{q}) \triangleq \Phi_{n-1}(\mathbf{p}, \mathbf{q}) \frac{\Xi_n(k_n)}{(\Lambda_n)^{i_n}} \frac{(q_n)^{i_n}}{i_n!} \frac{(p_n)^{l_n}}{l_n!} \times (\kappa_n - 1)! \frac{e^{-\frac{q_n}{\Lambda_n}}}{(\Lambda_n)^{-\kappa_n}}, \quad \forall n \geq 1. \quad (39)$$

Next, we consider delay-limited services at both C and E and resort to the outage probability to examine their performance. Let us define $R_{\text{th},C}$ as the target transmission rate of both $x_C^{[1]}$ and $x_C^{[2]}$, and $R_{\text{th},E}$ as that of both x_E and \hat{x}_E . If the instantaneous achievable rate falls below the corresponding target transmission rate, an outage event is said to occur. The end-to-end (e2e) outage probability (OP) of each UE is examined in the following subsections.

B. e2e OP of E

In this subsection, we examine the e2e OP of E, denoted as $\text{OP}_{E \rightarrow F}$. Since the transmission of x_E from E to F is assisted by the decode-and-forward (DF) UAV, the $\text{OP}_{E \rightarrow F}$ relies on the probability that U accurately decodes x_E , denoted as $\text{OP}_{E \rightarrow U}$. According to Algorithm 1, the event that U correctly decodes x_E is given by

$$\mathcal{S}^{[U]} = [\mathcal{E}_{C \rightarrow E}^{[U]}, \mathcal{S}_{C \rightarrow E}^{[U]}, \mathcal{S}_E^{[U]}] \text{ or } [\mathcal{E}_{E \rightarrow C}^{[U]}, \mathcal{S}_{E \rightarrow C}^{[U]}]. \quad (40)$$

Let us denote $\mathcal{S}_{E,C \rightarrow E}^{[U]} \triangleq [\mathcal{E}_{C \rightarrow E}^{[U]}, \mathcal{S}_{C \rightarrow E}^{[U]}, \mathcal{S}_E^{[U]}]$ and $\mathcal{S}_{E,E \rightarrow C}^{[U]} \triangleq [\mathcal{E}_{E \rightarrow C}^{[U]}, \mathcal{S}_{E \rightarrow C}^{[U]}]$, the OP at U can be formulated as

$$\text{OP}_{E \rightarrow U} = \Pr[\mathcal{S}^{[U]}] = 1 - \Pr[\mathcal{S}_{E,C \rightarrow E}^{[U]}] - \Pr[\mathcal{S}_{E,E \rightarrow C}^{[U]}]. \quad (41)$$

The OP at U comprises of two parts, $\Pr[\mathcal{S}_{E,C \rightarrow E}^{[U]}]$ and $\Pr[\mathcal{S}_{E,E \rightarrow C}^{[U]}]$, which corresponds to two possible decoding orders determined by $\mathcal{E}_{C \rightarrow E}^{[U]}$ and $\mathcal{E}_{E \rightarrow C}^{[U]}$, respectively. Accordingly, the ECFEs of $\varrho_1 \triangleq \Pr[\mathcal{S}_{E,C \rightarrow E}^{[U]}]$ and $\varrho_2 \triangleq \Pr[\mathcal{S}_{E,E \rightarrow C}^{[U]}]$ are provided by the following Lemmas. It is worth pointing out that ϱ_1 and ϱ_2 are the probabilities that U correctly decodes x_E when the C-U link is stronger and weaker than the E-U link, respectively.

Lemma 3. ECFE of ϱ_1 is given by

$$\varrho_1 = \sum_{K \geq k \geq 1} \sum_{\kappa \geq i \geq 0} \sum_{j+i=i} \Xi_2(k_2) \times \begin{cases} J_2 - J_1 - J_4 + J_3 \\ + J_5 - J_7 + J_8, & \text{if } \alpha_1 < 1, A_1 > a_2, \\ J_6, & \text{if } \alpha_1 < 1, A_1 \leq a_2, \\ J_2, & \text{if } \alpha_1 \geq 1, \end{cases} \quad (42)$$

where $\sum_{\kappa \geq i \geq 0} \equiv \sum_{j+i=i}^{\kappa_0-1} \sum_{j_0+l_0=i_0} \sum_{i_1=0}^{\kappa_1-1} \sum_{j_1+l_1=i_1}$, $\sum_{K \geq k \geq 1} \equiv \sum_{k_0=1}^{K_0+1} \sum_{k_1=1}^{K_1+1} \sum_{k_2=1}^{K_2+1}$, and

$$J_k \triangleq \frac{\Gamma\left(\kappa_2; \frac{q_2}{\Omega_2(k_2)} + \frac{q_2 p_1}{\Omega_1(k_1)} + \frac{q_2 p_1 p_0}{\Omega_0(k_0)}\right)}{\left(\frac{1}{\Omega_2(k_2)} + \frac{p_1}{\Omega_1(k_1)} + \frac{p_1 p_0}{\Omega_0(k_0)}\right)^{\kappa_2}} \times \Xi_0(k_0) \frac{(q_0)^{j_0} (p_0)^{l_0}}{j_0! l_0!} \Gamma(\kappa_0) \Xi_1(k_1) \frac{(q_1)^{j_1} (p_1)^{l_1}}{j_1! l_1!} \Gamma(\kappa_1) \times \frac{e^{-\frac{q_0}{\Omega_0(k_0)} - \frac{q_1}{\Omega_1(k_1)} - \frac{q_1 p_0}{\Omega_0(k_0)}}}{\left(\frac{1}{\Omega_1(k_1)} + \frac{p_0}{\Omega_0(k_0)}\right)^{\kappa_1 - i_0}} (\Lambda_0)^{\kappa_0 - i_0}, \quad (43)$$

where $k \in [0, 8]$ and the corresponding values for q_2 , p_1 , q_1 , p_0 , and q_0 are provided in Table I with $a_1 \triangleq \frac{\tau_{\text{th},C}}{\tilde{\gamma}_C(t_1)}$, $a_2 \triangleq \frac{\tau_{\text{th},E}}{\tilde{\gamma}_E(t_1)}$, $\alpha_1 \triangleq \frac{\tilde{\gamma}_E(t_1) \tau_{\text{th},C}}{\tilde{\gamma}_C(t_1)}$, $\alpha_2 \triangleq \frac{\tilde{\gamma}_C(t_1) \tau_{\text{th},E}}{\tilde{\gamma}_E(t_1)}$, $A_1 \triangleq \frac{a_1}{1 - \alpha_1}$, $A_2 \triangleq \frac{a_2}{1 - \alpha_2}$, and $\mathcal{A} \triangleq \frac{A_1 - a_2}{\alpha_2}$. Moreover, $K_n = 1$ for $n = 0, 1, 2$, and the values of $\chi_n(k_n)$, $\Omega_n(k_n)$, and $\mu_n(k_n)$ are given by Corollary 2 with $\hat{\gamma}_0 \sim \phi_{CU}$ and $\hat{\gamma}_1 \sim \phi_{EU}$, and by Corollary 3 with $\hat{\gamma}_2 \sim \varphi_{CU}$.

Proof: See Appendix B. ■

TABLE I
ARGUMENTS OF J_k , $1 \leq k \leq 8$.

	q_2	p_1	q_1	p_0	q_0		q_2	p_1	q_1	p_0	q_0
J_1	\mathcal{A}	α_2	a_2	α_1	a_1	J_5	\mathcal{A}	α_2	a_2	1	0
J_2	0	α_2	a_2	α_1	a_1	J_6	0	α_2	a_2	1	0
J_3	\mathcal{A}	0	A_1	α_1	a_1	J_7	\mathcal{A}	0	A_1	1	0
J_4	0	0	A_1	α_1	a_1	J_8	0	0	A_1	1	0

Lemma 4. *ECFE of ϱ_2 in (41) can be derived as*

$$\varrho_2 = \sum_{k_0=1}^{K_0+1} \sum_{k_1=1}^{K_1+1} \sum_{i_0=0}^{\kappa_0-1} \sum_{j_0+l_0=i_0} \Xi_1(k_1) \times \begin{cases} \hat{J}_2 - \hat{J}_1 + \mathbb{1}_{j_0} \hat{J}_3, & \text{if } \alpha_2 < 1, \\ \hat{J}_2, & \text{otherwise,} \end{cases} \quad (44)$$

where $\mathbb{1}_x = 1$ if $x = 0$, otherwise $\mathbb{1}_x = 0$,

$$\hat{J}_1 \triangleq \frac{\Gamma\left(\kappa_1; \frac{A_2}{\Omega_1(k_1)} + \frac{A_2 \alpha_2}{\Omega_0(k_0)}\right) \Xi_0(k_0) (a_2)^{j_0} (\alpha_2)^{l_0} \Gamma(\kappa_0)}{\left(\frac{1}{\Omega_1(k_1)} + \frac{\alpha_2}{\Omega_0(k_0)}\right)^{\kappa_1} j_0! l_0! (\Lambda_0)^{-\kappa_0 + i_0}} e^{-\frac{\alpha_2}{\Lambda_0}},$$

$$\hat{J}_2 \triangleq \frac{\Gamma(\kappa_1) \Xi_0(k_0)}{\left(\frac{1}{\Omega_1(k_1)} + \frac{\alpha_2}{\Omega_0(k_0)}\right)^{\kappa_1}} \frac{(a_2)^{j_0} (\alpha_2)^{l_0}}{j_0! l_0!} \Gamma(\kappa_0) (\Lambda_0)^{\kappa_0 - i_0} e^{-\frac{\alpha_2}{\Lambda_0}},$$

and

$$\hat{J}_3 \triangleq \frac{\Gamma\left(\kappa_1; \frac{A_2}{\Omega_1(k_1)} + \frac{A_2}{\Omega_0(k_0)}\right) \Xi_0(k_0) (\alpha_2)^{i_0}}{\left(\frac{1}{\Omega_1(k_1)} + \frac{1}{\Omega_0(k_0)}\right)^{\kappa_1} i_0!} \Gamma(\kappa_0) (\Lambda_0)^{\kappa_0 - i_0}.$$

In addition, we have $K_0 = K_1 = 1$, and the values of $\chi_n(k_n)$, $\Omega_n(k_n)$, and $\mu_n(k_n)$ are given by Corollary 2 with $\hat{\gamma}_0 \sim \phi_{EU}$ and $\hat{\gamma}_1 \sim \phi_{CU}$.

Proof: See Appendix C. ■

Now, let us define the e2e OP of E. Specifically, the proposed system adopts AMDs to decode the transmitted signal of E, where the event of correctly decoding E's information signal is formulated as

$$\mathcal{O}_E = \mathcal{S}_{E,U \rightarrow C} \text{ or } \mathcal{S}_{E,C \rightarrow U}, \quad (45)$$

where $\mathcal{S}_{E,U \rightarrow C} \triangleq [\mathcal{E}_{C \rightarrow U}^{[F]}, \mathcal{S}_{C \rightarrow U}^{[F]}, \mathcal{S}_U^{[F]}]$ and $\mathcal{S}_{E,C \rightarrow U} \triangleq [\mathcal{E}_{U \rightarrow C}^{[F]}, \mathcal{S}_{U \rightarrow C}^{[F]}]$.

After event $\mathcal{S}^{[U]}$ occurred, U forwards \hat{x}_E to F, and outage is declared when F incorrectly decodes \hat{x}_E . In addition, an outage is also declared when U remains silent. Therefore, the OP of E is composed of two parts as follows

$$\text{OP}_{E \rightarrow F} = \Pr[\bar{\mathcal{S}}^{[U]}] + \Pr[\mathcal{S}^{[U]}] \Pr[\bar{\mathcal{O}}_E | \mathcal{S}^{[U]}]. \quad (46)$$

Theorem 1. *The ECFE of e2e OP of E is obtained as*

$$\text{OP}_{E \rightarrow F} = 1 - (\varrho_1 + \varrho_2)(\varrho_3 + \varrho_4), \quad (47)$$

where ϱ_3 and ϱ_4 is analogous to ϱ_1 and ϱ_2 , respectively, by performing suitable substitutions. Specifically, we have $K_0 = m_{CF} - 1$, $K_1 = K_2 = 1$, and the values of $\chi_n(k_n)$, $\Omega_n(k_n)$, and $\mu_n(k_n)$ are given by Corollary 1-3, respectively, with $\hat{\gamma}_0 \sim \phi_{CF}$, $\hat{\gamma}_1 \sim \phi_{CU}$, and $\hat{\gamma}_2 \sim \varphi_{CF}$. Moreover, we have

$$\begin{aligned} a_1 &:= b_1, & A_1 &:= B_1, & \alpha_1 &:= \beta_1, \\ a_2 &:= b_2, & A_2 &:= B_2, & \alpha_2 &:= \beta_2, & \mathcal{A} &:= \mathcal{B}, \end{aligned} \quad (48)$$

with $b_1 \triangleq \frac{1}{\bar{\gamma}_C(t_2)} \tau_{\text{th},C}$, $b_2 \triangleq \frac{1}{\bar{\gamma}_U(t_2)} \tau_{\text{th},E}$, $\beta_1 \triangleq \bar{\gamma}_U(t_2) b_1$, $\beta_2 \triangleq \bar{\gamma}_C(t_2) b_2$, $B_1 \triangleq \frac{b_1}{1-\beta_1}$, $B_2 \triangleq \frac{b_2}{1-\beta_2}$ and $\mathcal{B} \triangleq \frac{B_1 - b_2}{\beta_2}$.

Proof: Following Algorithm 1 and (45), we obtain

$$\Pr[\mathcal{O}_E] = 1 - \Pr[\mathcal{S}_{C \rightarrow U}^{[F]}, \mathcal{S}_U^{[F]}, \mathcal{E}_{C \rightarrow U}^{[F]}] - \Pr[\mathcal{S}_{U \rightarrow C}^{[F]}, \mathcal{E}_{U \rightarrow C}^{[F]}], \quad (49)$$

where we find that $\varrho_3 \triangleq \Pr[\mathcal{S}_{C \rightarrow U}^{[F]}, \mathcal{S}_U^{[F]}, \mathcal{E}_{C \rightarrow U}^{[F]}]$ and $\varrho_4 \triangleq \Pr[\mathcal{S}_{U \rightarrow C}^{[F]}, \mathcal{E}_{U \rightarrow C}^{[F]}]$ can be derived in the same manner as ϱ_1 and ϱ_2 , respectively. Therefore we omit the detailed derivations for ϱ_3 and ϱ_4 from here. ■

C. e2e OPs of C

Recalling that C transmits different information during the first and second phases. According to Algorithm 1, the event that F correctly decodes $x_C^{[2]}$ depends on the outage event at U. Specifically, in the event $\mathcal{S}^{[U]}$, U correctly decodes $x_E(t_2)$, and can therefore cause interference at F due to the forwarded \hat{x}_E . In contrast, in the event $\bar{\mathcal{S}}^{[U]}$, F can directly decode $x_C^{[2]}$. Accordingly, the event that F correctly decodes $x_C^{[2]}$ can be formulated as

$$[\mathcal{S}^{[U]} \underbrace{(\mathcal{E}_{C \rightarrow U}^{[F]}, \mathcal{S}_{C \rightarrow U}^{[F]}) \cup (\mathcal{E}_{U \rightarrow C}^{[F]}, \mathcal{S}_{U \rightarrow C}^{[F]}, \mathcal{S}_C^{[F]})}_{\mathcal{X}}] \cup [\bar{\mathcal{S}}^{[U]} \mathcal{S}_C^{[2]}]. \quad (50)$$

Hence, the e2e OP of C in the second phase can be formulated as

$$\text{OP}_{C \rightarrow F}^{[2]} = \Pr[\mathcal{S}^{[U]}] \Pr[\chi] + \Pr[\bar{\mathcal{S}}^{[U]}] \Pr[\mathcal{S}_C^{[2]}]. \quad (51)$$

Theorem 2. *The ECFE of $\text{OP}_{C \rightarrow F}^{[2]}$ in (51) is obtained as*

$$\begin{aligned} \text{OP}_{C \rightarrow F}^{[2]} &= (\varrho_1 + \varrho_2)(1 - \varrho_5 - \varrho_6) \\ &\quad + (1 - \varrho_1 - \varrho_2)(1 - \varrho_7), \end{aligned} \quad (52)$$

where ϱ_7 is given by (57). Meanwhile, ϱ_5 and ϱ_6 is analogous to ϱ_1 and ϱ_2 , respectively, by performing suitable substitutions. Specifically, we have $K_0 = K_2 = 1$, $K_1 = m_{CF} - 1$, and the values of $\chi_n(k_n)$, $\Omega_n(k_n)$, and $\mu_n(k_n)$ are given by Corollary 1-3 with $\hat{\gamma}_0 \sim \phi_{UF}$, $\hat{\gamma}_1 \sim \phi_{CF}$, and $\hat{\gamma}_2 \sim \varphi_{UF}$, respectively. Moreover, we have

$$\begin{aligned} a_1 &:= b_2, & \alpha_1 &:= \beta_2, & A_1 &:= B_2, \\ a_2 &:= b_1, & \alpha_2 &:= \beta_1, & A_2 &:= B_1, & \mathcal{A} &:= \hat{\mathcal{B}}, \end{aligned} \quad (53)$$

with $\hat{\mathcal{B}} \triangleq \frac{B_2 - b_1}{\beta_1}$.

Proof: The probability $\Pr[\chi]$ can be derived as

$$\Pr[\chi] = 1 - \Pr[\mathcal{E}_{C \rightarrow U}^{[F]}, \mathcal{S}_{C \rightarrow U}^{[F]}] - \Pr[\mathcal{E}_{U \rightarrow C}^{[F]}, \mathcal{S}_{U \rightarrow C}^{[F]}, \mathcal{S}_C^{[F]}], \quad (54)$$

where we find that $\varrho_5 \triangleq \Pr[\mathcal{E}_{C \rightarrow U}^{[F]}, \mathcal{S}_{C \rightarrow U}^{[F]}]$ and $\varrho_6 \triangleq \Pr[\mathcal{E}_{U \rightarrow C}^{[F]}, \mathcal{S}_{U \rightarrow C}^{[F]}, \mathcal{S}_C^{[F]}]$ can be derived in the same manner as ϱ_1 and ϱ_2 , respectively. Therefore we omit the detailed derivations for ϱ_5 and ϱ_6 from the proof.

For $\varrho_7 \triangleq \Pr[\mathcal{S}_C^{[2]}]$, we have

$$\varrho_7 = \Pr \left[g_{CF}^2 < \frac{\frac{1}{\bar{\gamma}_C(t_2)} \tau_{\text{th},C}}{\mathcal{L}_{CF}} \right] = \int_0^{\frac{\frac{1}{\bar{\gamma}_C(t_2)} \tau_{\text{th},C}}{\mathcal{L}_{CF}}} f_{g_{CF}^2}(t) dt. \quad (55)$$

It is noted that

$$\begin{aligned} F_{|h_{CF}|^2}(x) &= \int_0^{\frac{x}{\mathcal{L}_{CF}}} f_{g_{CF}^2}(t) dt = \alpha \left(1 - e^{-\frac{\beta - \delta}{\mathcal{L}_{CF}} x} \right) \\ &\quad + \alpha \sum_{l=1}^{m_{CF}-1} \frac{\zeta(l)}{l!} \gamma \left(l+1; \frac{\beta - \delta}{\mathcal{L}_{CF}} x \right) \left(\frac{\beta - \delta}{\mathcal{L}_{CF}} \right)^{-l-1}, \end{aligned} \quad (56)$$

Hence, (55) can derived as

$$\varrho_7 = F_{|h_{CF}|^2}(b_1), \quad (57)$$

where $b_1 := \frac{1}{\bar{\gamma}_C(t_2)} \tau_{\text{th},C}$.

Finally, utilizing the foregoing results, we can re-express $\text{OP}_{F, x_C^{[2]}}$ as a function of ϱ_1 , ϱ_2 , ϱ_5 , ϱ_6 and ϱ_7 . This completes the proof of Theorem 2. ■

Theorem 3. Let us denote $\text{OP}_{\text{C} \rightarrow \text{F}}^{[1]}$ as the e2e OP of C in the first phase, which is defined as the probability of failing to decode $x_{\text{C}}^{[1]}$; we have

$$\text{OP}_{\text{C} \rightarrow \text{F}}^{[1]} = \varrho_8, \quad (58)$$

where $\varrho_8 \triangleq F_{|h_{\text{CF}}|^2}(a_1)$ with $a_1 := \frac{1}{\bar{\gamma}_{\text{C}}(t_1)} \tau_{\text{th}, \text{C}}$.

Proof: Following the Algorithm 1, the OP at F when decoding $x_{\text{C}}^{[1]}$ can be formulated as $\text{OP}_{\text{C} \rightarrow \text{F}}^{[1]} = \Pr[\mathcal{S}_{\text{C}}^{[1]}]$. Plugging (12) into the above equation, and after some mathematical steps, we obtain

$$\text{OP}_{\text{C} \rightarrow \text{F}}^{[1]} = \Pr \left[g_{\text{CF}}^2 < \frac{\frac{1}{\bar{\gamma}_{\text{C}}(t_1)} \tau_{\text{th}, \text{C}}}{\mathcal{L}_{\text{CF}}} \right] = \int_0^{\frac{\frac{1}{\bar{\gamma}_{\text{C}}(t_1)} \tau_{\text{th}, \text{C}}}{\mathcal{L}_{\text{CF}}}} f_{g_{\text{CF}}^2}(t) dt, \quad (59)$$

which is similar to (55), thus resulting in (58). This completes the proof of Theorem 3. \blacksquare

D. Non-adaptive decoding mechanism

We discuss non-ADM (NADMs) in this subsection. In the case of 2-user CDRT-NOMA, there are four alternative non-adaptive decoding orders, denoted as $\mathbf{D}_n = (i, j)$ with $n \in \{1, 2, 3, 4\}$, where $i, j \in \{\text{E}, \text{C}\}$. Hence, $\mathbf{D}_1 = (\text{C}, \text{C})$, $\mathbf{D}_2 = (\text{E}, \text{C})$, $\mathbf{D}_3 = (\text{C}, \text{E})$, and $\mathbf{D}_4 = (\text{E}, \text{E})$.

In the first and the second NADMs, where F first decodes C's information signal before decoding x_{E} , the e2e OPs of C, in the second phase, and E are obtained as

$$\text{OP}_{\text{C} \rightarrow \text{F}}^{[2]}(\mathbf{D}_n) = \Pr[\bar{\mathcal{S}}_i^{[\text{U}]} \bar{\mathcal{S}}_{\text{C} \rightarrow \text{U}}^{[\text{F}]}] + \Pr[\bar{\mathcal{S}}_i^{[\text{U}]} | \bar{\mathcal{S}}_{\text{C}}^{[2]}], \quad (60)$$

$$\text{OP}_{\text{E} \rightarrow \text{F}}(\mathbf{D}_n) = \Pr[\bar{\mathcal{S}}_i^{[\text{U}]}] + \Pr[\bar{\mathcal{S}}_i^{[\text{U}]}] \Pr[\bar{\mathcal{S}}_{\text{C} \rightarrow \text{U}}^{[\text{F}]} \cup \bar{\mathcal{S}}_{\text{U}}^{[\text{F}]} | \bar{\mathcal{S}}_i^{[\text{U}]}], \quad (61)$$

respectively, where $\bar{\mathcal{S}}_{\text{C}}^{[\text{U}]} \triangleq [\mathcal{S}_{\text{C} \rightarrow \text{E}}^{[\text{U}]} \mathcal{S}_{\text{E}}^{[\text{U}]}]$, and $\bar{\mathcal{S}}_{\text{E}}^{[\text{U}]} \triangleq [\mathcal{S}_{\text{E} \rightarrow \text{C}}^{[\text{U}]}]$. It is noted that the first NADM is often utilized in cellular networks, here cell-center users are assumed to yield better channel power gains and thus should not be treated as interference in the decoding of x_{E} to avoid frequent outages.

Moreover, in the third and fourth NADMs, where F decodes \hat{x}_{E} before decoding $x_{\text{C}}^{[2]}$, the e2e OPs C, in the second phase, and E are obtained as

$$\begin{aligned} \text{OP}_{\text{C} \rightarrow \text{F}}^{[2]}(\mathbf{D}_n) &= \Pr[\bar{\mathcal{S}}_i^{[\text{U}]} | \bar{\mathcal{S}}_{\text{C} \rightarrow \text{U}}^{[\text{F}]}] \\ &\quad + \Pr[\bar{\mathcal{S}}_i^{[\text{U}]}] \Pr[\bar{\mathcal{S}}_{\text{U} \rightarrow \text{C}}^{[\text{F}]} \cup \bar{\mathcal{S}}_{\text{C}}^{[\text{F}]} | \bar{\mathcal{S}}_i^{[\text{U}]}], \end{aligned} \quad (62)$$

$$\text{OP}_{\text{E} \rightarrow \text{F}}(\mathbf{D}_n) = \Pr[\bar{\mathcal{S}}_i^{[\text{U}]}] + \Pr[\bar{\mathcal{S}}_i^{[\text{U}]}] \Pr[\bar{\mathcal{S}}_{\text{U} \rightarrow \text{C}}^{[\text{F}]} | \bar{\mathcal{S}}_i^{[\text{U}]}], \quad (63)$$

respectively.

IV. OPTIMAL POWER ALLOCATION

In this section, we formulate and propose a solution to the system throughput maximization problem.

Corollary 4. Based on Theorems 1-3, the system throughput can be formulated as follows

$$\begin{aligned} \mathcal{R}_{\Sigma}(\mathbf{p}) &= \frac{R_{\text{th}, \text{C}}}{2} [1 - \text{OP}_{\text{C} \rightarrow \text{F}}^{[1]}(P_{\text{C}}^{[1]}, P_{\text{E}}, P_{\text{U}}, P_{\text{C}}^{[2]})] \\ &\quad + \frac{R_{\text{th}, \text{E}}}{2} [1 - \text{OP}_{\text{E} \rightarrow \text{F}}(P_{\text{C}}^{[1]}, P_{\text{E}}, P_{\text{U}}, P_{\text{C}}^{[2]})] \\ &\quad + \frac{R_{\text{th}, \text{C}}}{2} [1 - \text{OP}_{\text{C} \rightarrow \text{F}}^{[2]}(P_{\text{U}}, P_{\text{C}}^{[2]})]. \end{aligned} \quad (64)$$

Algorithm 2: Proposed Iterative Numerical Gradient Descend-based Algorithm for finding \mathcal{R}_{Σ}^*

- 1 **initialize:** iteration index $k \leftarrow 0$, randomize starting points $\theta_1^{(k)} \in [0, 1]$ and $\theta_2^{(k)} \in [0, 1]$, step size $\tau \leftarrow 0.05$, numerical accuracy $\eta \leftarrow 10^{-4}$, and error tolerance $\varrho \leftarrow 0.0025$.
 - 2 **repeat**
 - 3 Compute: $\mathcal{R}_0^{(k)} \leftarrow \mathcal{R}_{\Sigma}(\boldsymbol{\theta}^{(k)})$;
 - 4 Compute: $\mathcal{R}_1^{(k)} \leftarrow \mathcal{R}_{\Sigma}(\theta_1^{(k)} + 0_{\text{E}}, \theta_2^{(k)})$;
 - 5 Compute: $\mathcal{R}_2^{(k)} \leftarrow \mathcal{R}_{\Sigma}(\theta_1^{(k)}, \theta_2^{(k)} + 0_{\text{E}})$;
 - 6 Compute: $\frac{\partial \mathcal{R}_{\Sigma}}{\partial \theta_1}(\boldsymbol{\theta}^{(k)}) \leftarrow \frac{1}{0_{\text{E}}}(\mathcal{R}_1^{(k)} - \mathcal{R}_0^{(k)})$;
 - 7 Compute: $\frac{\partial \mathcal{R}_{\Sigma}}{\partial \theta_2}(\boldsymbol{\theta}^{(k)}) \leftarrow \frac{1}{0_{\text{E}}}(\mathcal{R}_2^{(k)} - \mathcal{R}_0^{(k)})$;
 - 8 Compute: $(\nabla_{\boldsymbol{\theta}} \mathcal{R}_{\Sigma})(\boldsymbol{\theta}^{(k)}) \leftarrow \begin{bmatrix} \frac{\partial \mathcal{R}_{\Sigma}}{\partial \theta_1}(\boldsymbol{\theta}^{(k)}) \\ \frac{\partial \mathcal{R}_{\Sigma}}{\partial \theta_2}(\boldsymbol{\theta}^{(k)}) \end{bmatrix}$;
 - 9 Update: $\boldsymbol{\theta}^{(k+1)} \leftarrow \boldsymbol{\theta}^{(k)} + \tau(\nabla_{\boldsymbol{\theta}} \mathcal{R}_{\Sigma})(\boldsymbol{\theta}^{(k)})$;
 - 10 Update: $k \leftarrow k + 1$;
 - 11 **until** $\|(\nabla_{\boldsymbol{\theta}} \mathcal{R}_{\Sigma})(\boldsymbol{\theta}^{(k)})\|_2 < \varrho$;
 - 12 **output:** $\boldsymbol{\theta}^* = \boldsymbol{\theta}^{(k)}$ and $\mathcal{R}_{\Sigma}^* = \mathcal{R}_{\Sigma}(\boldsymbol{\theta}^*)$.
-

First, we formalize the problem as follows

$$\begin{aligned} &\underset{\mathbf{p}}{\text{maximize}} && \mathcal{R}_{\Sigma} \\ &\text{subject to} && C_1 : P_{\text{C}}^{[1]} + P_{\text{E}} \leq P_{\text{max}}^{[1]}, \\ & && C_2 : P_{\text{U}} + P_{\text{C}}^{[2]} \leq P_{\text{max}}^{[2]}, \end{aligned} \quad (65)$$

where $\mathbf{p} \triangleq [P_{\text{C}}^{[1]}, P_{\text{E}}, P_{\text{U}}, P_{\text{C}}^{[2]}]^T$. Constraints C_1 and C_2 indicate that the total transmit power of transmitters should not be larger than the power budget in the first and the second time-slots, respectively.

From (65), C_1 and C_2 always hold for the optimal solution. Subsequently, the transmit powers can be expressed as $P_{\text{C}}^{[1]} = \theta_1 P_{\text{max}}^{[1]}$, $P_{\text{E}} = (1 - \theta_1) P_{\text{max}}^{[1]}$, $P_{\text{C}}^{[2]} = \theta_2 P_{\text{max}}^{[2]}$, and $P_{\text{U}}(t_1) = (1 - \theta_2) P_{\text{max}}^{[2]}$, where $\theta_1 \triangleq \frac{P_{\text{C}}^{[1]}}{P_{\text{C}}^{[1]} + P_{\text{E}}} \triangleq \frac{P_{\text{C}}^{[1]}}{P_{\text{max}}^{[1]}}$, $\theta_2 \triangleq \frac{P_{\text{C}}^{[2]}}{P_{\text{U}} + P_{\text{C}}^{[2]}} = \frac{P_{\text{C}}^{[2]}}{P_{\text{max}}^{[2]}}$. Accordingly, the optimization problem in (65) can be reformulated as

$$\begin{aligned} &\underset{\theta_1, \theta_2}{\text{maximize}} && \mathcal{R}_{\Sigma}(\theta_1, \theta_2) \\ &\text{subject to} && 0 \leq \theta_1 \leq 1, \\ & && 0 \leq \theta_2 \leq 1. \end{aligned} \quad (66)$$

where

$$\begin{aligned} \mathcal{R}_{\Sigma}(\theta_1, \theta_2) &= \frac{R_{\text{th}, \text{C}}}{2} [1 - \text{OP}_{\text{C} \rightarrow \text{F}}^{[1]}(\theta_1, \theta_2) + 1 - \text{OP}_{\text{C} \rightarrow \text{F}}^{[2]}(\theta_2)] \\ &\quad + \frac{R_{\text{th}, \text{E}}}{2} [1 - \text{OP}_{\text{E} \rightarrow \text{F}}(\theta_1, \theta_2)]. \end{aligned} \quad (67)$$

In order to find the optimal solution to the above problem, derivative-based algorithms, such as the Gradient Descend, can be utilized. In order to perform Gradient Descend, we need to calculate the gradient $\nabla \mathcal{R}_{\Sigma}$ by performing the derivatives of $\mathcal{R}_{\Sigma}(\theta_1, \theta_2)$ with respect to (w.r.t.) θ_1 and θ_2 . We thus need to determine $\frac{\partial}{\partial \theta_1} \text{OP}_{\text{E} \rightarrow \text{F}}$, $\frac{\partial}{\partial \theta_1} \text{OP}_{\text{C} \rightarrow \text{F}, t_1}$, $\frac{\partial}{\partial \theta_1} \text{OP}_{\text{C} \rightarrow \text{F}, t_2}$, $\frac{\partial}{\partial \theta_2} \text{OP}_{\text{E} \rightarrow \text{F}}$, $\frac{\partial}{\partial \theta_2} \text{OP}_{\text{C} \rightarrow \text{F}, t_1}$, and $\frac{\partial}{\partial \theta_2} \text{OP}_{\text{C} \rightarrow \text{F}, t_2}$. Therefore, it

will require an excessive number of derivatives to obtain $\nabla \mathcal{R}_\Sigma$. For instance, the derivatives $\frac{\partial}{\partial \theta_1} \text{OP}_{E \rightarrow F}$ can be obtained as

$$\begin{aligned} \frac{\partial}{\partial \theta_1} \text{OP}_{E \rightarrow F} = & -\text{Pr}[0_E] \cdot \frac{\partial}{\partial \theta_1} \text{Pr}[S^{[U]}] \\ & - \text{Pr}[S^{[U]}] \cdot \frac{\partial}{\partial \theta_1} \text{Pr}[0_E]. \end{aligned} \quad (68)$$

Since $\text{Pr}[0_E]$ is calculated via the events in the second phase, i.e., $E_{C \rightarrow U}^{[F]}$, $S_{C \rightarrow U}^{[F]}$, $S_U^{[F]}$, $E_{U \rightarrow C}^{[F]}$, and $S_{U \rightarrow C}^{[F]}$, it is independent of θ_1 (i.e., the power allocation in the first phase) thus $\frac{\partial}{\partial \theta_1} \text{OP}_{F, x_E}$ can be rewritten as

$$\frac{\partial}{\partial \theta_1} \text{OP}_{E \rightarrow F} = -\text{Pr}[0_E] \cdot \frac{\partial}{\partial \theta_1} \text{Pr}[S^{[U]}]. \quad (69)$$

Calculating the derivative of $\text{Pr}[S^{[U]}]$ requires the derivatives of J_i for $1 \leq i \leq 8$, and J'_j for $j = 1, 2, 3$. In addition, since J_i is a multi-variate function of q_2, p_1, q_1, p_0 , and q_0 , and J'_j is a multi-variate function of q_1, p_0 , and q_0 , a total of $5 \times 8 + 3 \times 3 = 49$ derivatives are required to determine $\frac{\partial}{\partial \theta_1} \text{Pr}[0_E]$. To overcome this mundane, we propose a Gradient Descend-inspired algorithm in Table 2. In this algorithm, we perform traditional Gradient descend to find θ^* and $\mathcal{R}_\Sigma(\theta^*)$, which represent the optimal UL power allocation and the optimal throughput, respectively. During each k -th iteration, instead of analytically calculating the Gradient of \mathcal{R}_Σ , we numerically evaluate $\nabla \mathcal{R}_\Sigma$, as in Step 3 of Algorithm 2, by adopting the following identity

$$\frac{f(x + \eta) - f(x)}{\eta} \rightarrow \frac{\partial f}{\partial x}(x), \quad (70)$$

where $\eta > 0$ represents the numerical accuracy satisfying

$$|f(x + \eta) - f(x)| > 0. \quad (71)$$

Then, the power allocation is updated for the next iteration as in Step 4, where $\theta^{(k)} = [\theta_1^{(k)}, \theta_2^{(k)}]^T$. The algorithm iterates until the stopping criterion in Step 6 is satisfied.

V. NUMERICAL RESULTS

This section includes numerical results to validate the correctness of the analysis provided in previous sections. Furthermore, with the obtained results, we provide additional insights on the performance of the proposed UAV-aided double uplink system. In what follows, unless otherwise specified, the simulation settings are those that are provided in Table II.

In Fig. 2, we consider that U can move following a random waypoint (RWP) mobility model within a 2D circular area A parallel to the xy -plane of the 3D Cartesian coordinate system. The area A has radius $R_A = \frac{|\mathbf{p}_C - \mathbf{p}_E|}{2}$ and is centered on the initial location of U, \mathbf{p}_U , so that U always lies between E and F. Let us denote \mathbf{p}_i as the coordinate of the i -th waypoint that U chooses in movement period i . The movement trace of U can be modeled as a discrete-time stochastic process, given by $\{\mathbf{p}_i\}_{i \in \mathbb{N}} = \{\mathbf{p}_1, \mathbf{p}_2, \mathbf{p}_3, \dots\}$. The waypoints $\mathbf{p}_1, \mathbf{p}_2, \mathbf{p}_3, \dots$, are random variables that are chosen to be mutually independent and identically distributed (i.i.d) and are uniformly distributed over A . U moves from the initial waypoint \mathbf{p}_i to the next waypoint \mathbf{p}_{i+1} as follows. First, U

TABLE II
SIMULATION PARAMETERS

Parameter	Value
Maximum network dimension [m]	50
Target spectral efficiency of C [bits/s/Hz]	1.0
Residual interference level [dB]	-10
Target spectral efficiency of E [bits/s/Hz]	0.05
Transmit Antenna gains [dBi]	0
Carrier frequency, f_c [GHz]	3
Receive Antenna gains [dBi]	0
LoS Link attenuation, η , [dB]	1.6
Bandwidth, BW [MHz]	20
NLoS Link attenuation, $\bar{\eta}$, [dB]	23
Noise power density, σ^2 [dBm/Hz]	-144
LoS fading severity, $m_{CF}, m_{CU}, m_{EU}, m_{UF}$	5, 3, 1, 5

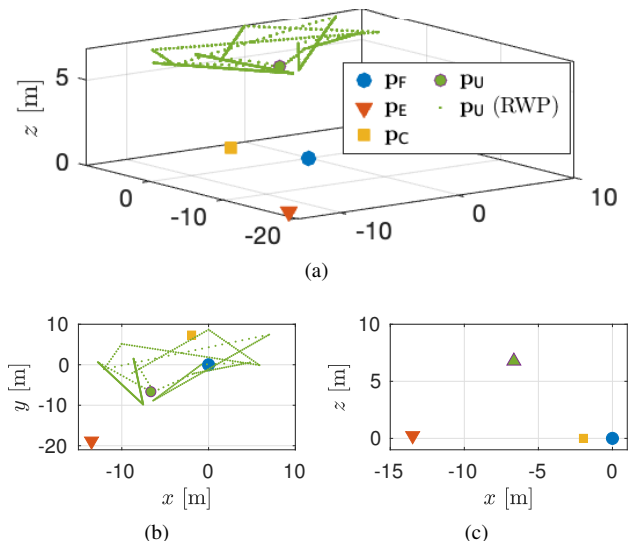


Fig. 2. Top-down view of 10^3 locations of U captured by RWM model, where (a) 3D view of the network topology, (b) projection of (a) on the xy -plane, and (c) projection of (a) on the xz -plane, when $\mathbf{p}_F = (0, 0, 0)$, $\mathbf{p}_C = (-1.96, 7.33, 0)$, $\mathbf{p}_E = (-13.49, -18.85, 0.23)$, and $\mathbf{p}_U = (-6.66, -7.62, 6.77)$.

chooses a new speed $V_i \in [v_{\min}, v_{\max}]$. Then, U moves along the line segment from \mathbf{p}_i to \mathbf{p}_{i+1} in the direction

$$\psi_{i \rightarrow i+1} = \text{sgn}(Y_{i+1} - Y_i) \arccos \frac{X_{i+1} - X_i}{|\mathbf{p}_{i+1} - \mathbf{p}_i|}, \quad (72)$$

with the constant velocity V_i until U reaches \mathbf{p}_{i+1} . In (72), $\text{sgn}(x)$ denotes the sign function. The location of U at time $(t+1)$ can be formulated as

$$X_U(t+1) = X_U(t) + V_i \sin \psi_{i \rightarrow i+1} \quad (73)$$

$$Y_U(t+1) = Y_U(t) + V_i \cos \psi_{i \rightarrow i+1}. \quad (74)$$

Then, U pauses for a duration of T_i at the waypoint \mathbf{p}_{i+1} . In this simulation, we assume that $T_i = 0$, and V_i is uniformly distributed within the interval $[v_{\min}, v_{\max}]$ with $v_{\min} = 0.1$ and $v_{\max} = 1$.

Impact on P_{\max} to the e2e OPs: In Fig. 3, we compare the e2e OP of E and C with the proposed ADM for UAV-aided coordinated D-UL systems with different target spectral efficiency pairs; i.e., $\mathbf{R}_1 = (2, 0.1)$ bits/s/Hz, $\mathbf{R}_2 = (1, 0.05)$ bits/s/Hz, and $\mathbf{R}_3 = (0.5, 0.025)$ bits/s/Hz, where

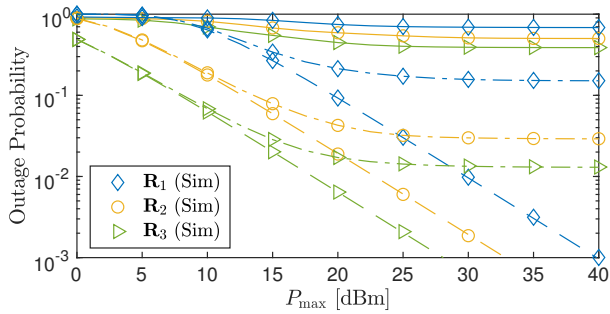


Fig. 3. Impact of the maximum power budget, P_{\max} , on $OP_{E \rightarrow F}$ (solid), $OP_{C \rightarrow F}^{[1]}$ (dashed), $OP_{C \rightarrow F}^{[2]}$ (dot-dash).

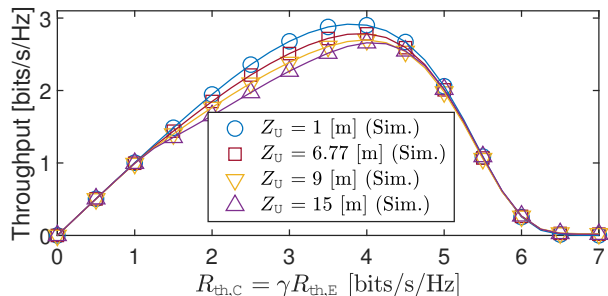


Fig. 4. Throughput versus the target SE and U's altitude (i.e., Z_U).

$\mathbf{R}_j \triangleq (R_{th,C}, R_{th,E})$. It is observed that the simulation results match the analytical results, which validate our analysis.

Under the proposed ADM, it is shown that $OP_{E \rightarrow F}$, $OP_{C \rightarrow F}^{[2]}$, and $OP_{C \rightarrow F}^{[1]}$ decrease as P_{\max} increases where

$$OP_{E \rightarrow F} \geq OP_{C \rightarrow F}^{[2]} \geq OP_{C \rightarrow F}^{[1]}. \quad (75)$$

This can be explained as follows. Due to imperfect SIC, the decoding of x_E involves co-channel interference (CCI) terms $(1 - \theta_1)P_{\max}g_{EU}^2\mathcal{L}_{EU}$ and $\theta_1P_{\max}|\tilde{h}_{CU}|^2$, and that of \hat{x}_E involves interference power of $\theta_1P_{\max}g_{CU}^2\mathcal{L}_{CU}$. Moreover, the decoding of $x_C^{[2]}$ suffers from the interference from $(1 - \theta_2)P_{\max}g_{UF}^2\mathcal{L}_{UF}$ and the RI $(1 - \theta_2)P_{\max}|\tilde{h}_{UF}|^2$. Meanwhile, F can directly decode $x_C^{[1]}$ without being affected by the CCIs, which results in the lowest e2e OP as in (75). Another observation from Fig. 3 is that the outage performance can be improved by reducing $R_{th,C}$ and/or $R_{th,E}$. Specifically, by halving both $R_{th,C}$ and $R_{th,E}$, from 2.0 bits/s/Hz to 1.0 bits/s/Hz and from 0.1 bits/s/Hz to 0.5 bits/s/Hz, respectively, $OP_{E \rightarrow F}$, $OP_{C \rightarrow F}^{[1]}$, and $OP_{C \rightarrow F}^{[2]}$ at $P_{\max} = 35$ dBm decrease from $10^{-2.8}$, $10^{-1.8}$, and $10^{-0.5}$ to $10^{-3.9}$, $10^{-1.95}$, and $10^{-0.8}$, respectively. In this case, the QoS requirements become less demanding, thus decreasing the e2e OPs. In other words, the e2e OPs are increasing functions of the target spectral efficiency, i.e., $R_{th,E}$ and $R_{th,C}$.

Impact of $R_{th,C}$ and $R_{th,E}$ on the system throughput: In Fig. 4, we illustrate the throughput versus $R_{th,C}$ and $R_{th,E}$, when γ is set to 20. It is observed that as $R_{th,C}$ increases above 0 bits/s/Hz, the throughput gradually increases until reaching peak values. For instance, the peak value of throughput when U is located at the altitude $Z_U = 6.67$ [m] is 2.75 bits/s/Hz. Beyond that value, the throughput drastically drops to 0

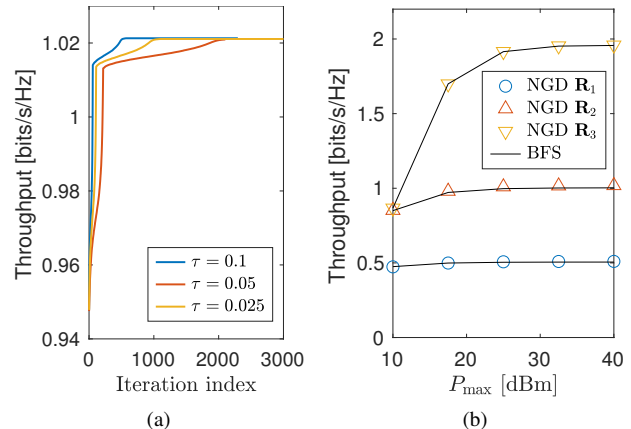


Fig. 5. (a) The convergence speed of the numerical gradient descend-based (NGD) algorithm and (b) performance comparison between the brute-force search (BFS) and NGD algorithms.

bits/s/Hz. The reason for this is because while the proposed ADM can satisfy a wide variety of QoS requirements, they cannot meet higher demands of ground users, which leads to a drastic decrease in the system throughput.

Numerical Gradient Descend-based Algorithm: In Figs. 5a and 5b, we examine the accuracy of the obtained optimal power allocation coefficients using the proposed NGD-based algorithm. As can be seen in Fig. 5a, the NGD-based algorithm converges to the optimal point. The step τ has strong impact on the convergence speed, the higher τ , the faster convergence the algorithm can reach. In Fig. 5b, we show that the proposed NGD-based algorithm results in similar optimal throughput as that achieved by the BFS algorithm, and the optimality gap between the two algorithms is relatively small. Specifically, let us define the mean squared error (MSE) as $MSE \triangleq \frac{1}{N} \sum_{n=1}^N \left| \mathcal{R}_{\Sigma}^{*,BFS}(\mathbf{p}_U[n]) - \mathcal{R}_{\Sigma}^{*,NGD}(\mathbf{p}_U[n]) \right|^2$, where N denotes the number of data points, $\mathcal{R}_{\Sigma}^{*,BFS}[n]$, and $\mathcal{R}_{\Sigma}^{*,NGD}[n]$ are the optimal and sub-optimal system throughput obtained from the BFS and the NGD at the n -th data point, respectively. It can be observed that the proposed algorithm matches well with the BFS algorithm, with an MSE of 4.2583×10^{-8} over $N = 10^2$ data points.

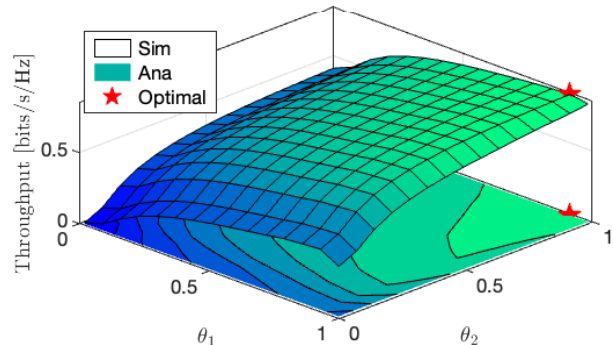


Fig. 6. Throughput at the initial location of U as a function of θ_1 and θ_2 .

Impact of θ_1 and θ_2 on the system throughput: In Fig. 6,

we examine the system throughput in (67) versus the power allocation in the first and the second phase, i.e., θ_1 and θ_2 , respectively. The optimal value is obtained by using the brute-force search algorithm. In addition, it can be observed that as θ_1 and θ_2 increase from zero to one, more power is allocated to both $x_C^{[1]}$ and $x_C^{[2]}$, and the throughput increases to the optimal value, which is marked by the red star. Beyond the optimal value, less power is allocated to x_E and \hat{x}_E , thus causing a slight drop in the system throughput.

Impact of Θ_U on the outage performance: In Fig. 7, we

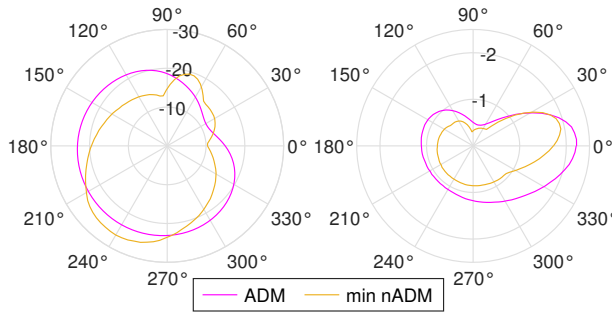


Fig. 7. Impact of Θ_U [deg] to a) $OP_{C \rightarrow F}^{[2]}$, and b) $OP_{E \rightarrow F}$.

compare the e2e OPs of the proposed ADM to that of the NADMs. The yellow curves in Figs. 7(a) and 7(b) are defined as

$$OP_{C \rightarrow F, t_2}^* = \min_{1 \leq n \leq 4} [OP_{C \rightarrow F}^{[2]}(\mathbf{D}_n)],$$

$$OP_{E \rightarrow F}^* = \min_{1 \leq n \leq 4} [OP_{E \rightarrow F}(\mathbf{D}_n)],$$

respectively, which depict the minimum OPs of the aforementioned NADMs. It can be observed that $OP_{C \rightarrow F}^{[2]} \geq OP_{C \rightarrow F, t_2}^*$ when Θ_U ranges from 210° to 270° and from 30° to 90° . However, in both Fig. 7(a) and Fig. 7(b), $OP_{C \rightarrow F}^{[2]}$ and $OP_{E \rightarrow F}$ cover the majority of $OP_{C \rightarrow F, t_2}^*$ and $OP_{E \rightarrow F}^*$, respectively, which implies that, in certain locations, the proposed ADM slightly performs worse than the NADMs in terms of OPs.

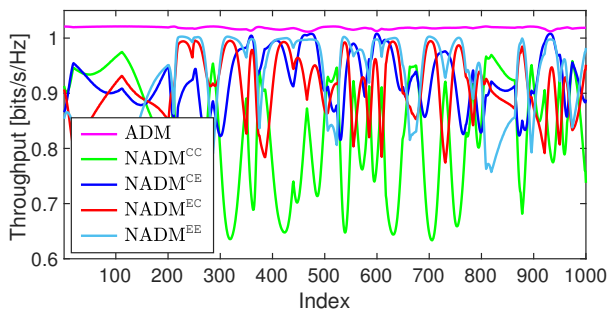


Fig. 8. ADM vs NADMs over multiple locations of U according to the RWP mobility model, where a) illustrate the optimal throughput at 300 locations of U, and b) show the throughput at 3000 random locations of U, where the residual level is at -30 dB.

Impact of the locations of U: In Fig. 8, we compare the system throughput of the proposed ADM to that of the conventional NADMs. It can be observed that the ADM provides a stable system throughput, which maintains \mathcal{R}_Σ around 1.25 bits/s/Hz even if U moves following the trajectory

in Fig. 2(a). In contrast, with NADMs, the system throughput wildly fluctuates and becomes unpredictable. For instance, the conventional NADM(1) (i.e., the green line) causes the system throughput to fluctuate between 0.65 bit/s/Hz to 0.95 bits/s/Hz. This is because when U moves, the path losses between the wireless nodes (i.e., \mathcal{L}_{CU} , \mathcal{L}_{EU} , \mathcal{L}_{UF} , and \mathcal{L}_{CF}) also fluctuates rapidly. In this context, U and F cannot adaptively adjust the decoding order according to this fluctuation, thus resulting in unpredictable outage behaviors. Since the system throughput, in this paper, is based on the e2e OPs, the throughput obtained using NADMs also fluctuates significantly.

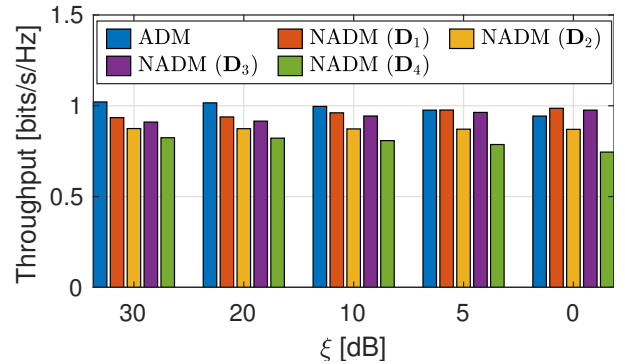


Fig. 9. Throughput of ADM and NADM versus the RI level at U and F, when $\xi_U = \xi_F = \xi$.

Impact of the residual interference level: In Fig. 9, we study the impact of the RI level on the system throughput of the proposed UAV-aided double uplink system. It can be observed that when ξ increases from -30 dB to 0 dB, the throughput decreases for both ADM and NADMs. However, the throughput does not necessarily reach zero when $\xi = 0$ dB. This is because the decoding of x_E , $x_C^{[2]}$, and \hat{x}_E are affected by the RI power from $P_C^{[1]}|\tilde{h}_{CU}|^2$, $P_C^{[2]}|\tilde{h}_{CF}|^2$, and $P_U|\tilde{h}_{UF}|^2$. Thus, as ξ increases, the RI power increases, reducing the system throughput. However, the decoding of $x_C^{[2]}$ is not affected by the RI power, thus resulting in a lower bound for the system throughput, such that

$$\mathcal{R}_\Sigma(\xi) \geq \frac{R_{th,C}}{2}(1 - OP_{C \rightarrow F}^{[1]}), \quad \forall \xi \in [0, 1], \quad (76)$$

which ensures the proposed system also provides an acceptable throughput, even in the presence of high RI powers.

VI. CONCLUSION

In this paper, we proposed ADM for UAV-aided D-UL CDRT-NOMA networks. Specifically, by exploiting the channel gains from the transmitters (i.e., the terrestrial users and U) the proposed ADM decide on the decoding order at the receivers in an adaptive manner. To evaluate the performance of the proposed mechanisms, we derived exact closed-form expressions for the e2e OP and system throughput. We showed that the proposed ADM can provide better performance in terms of OPs and throughput than the traditional NADMs. To study the impact of U's trajectory, we modelled the locations of U over time using the RWM model, and showed that the proposed ADM can maintain the system throughput regardless

of the locations of U. In contrast, the performance of the NADMs significantly fluctuate over the locations of U. To study the optimal throughput, we proposed a sub-optimal Gradient Descent-based algorithm and compare it to the BFS algorithm. The results show that the proposed sub-optimal algorithm matches to BFS algorithm.

APPENDIX A PROOF OF LEMMA 2

Using (25) and applying [28, Eq. (8.352.2)], we get $\Gamma(n, x) = \Gamma(n)e^{-x} \sum_{k=0}^{n-1} \frac{x^k}{k!}$, the integral I_0 can then be obtained as

$$I_0 = \sum_{k_0=1}^{K_0+1} \chi_0(k_0) e^{-\frac{p_0 x_1 + q_1}{\Lambda_0}} \sum_{i_0=0}^{\kappa_0-1} \frac{\left(\frac{p_0 x_1 + q_1}{\Lambda_0}\right)^{i_0}}{i_0!}. \quad (77)$$

Subsequently, by applying the binomial theorem, we get

$$\left(\frac{p_0 x_1 + q_1}{\Lambda_0}\right)^{i_0} = \frac{i_0!}{(\Lambda_0)^{i_0}} \sum_{j_0+l_0=i_0} \frac{(p_0 x_1)^{l_0}}{l_0!} \frac{(q_0)^{j_0}}{j_0!}$$

and utilizing (25), the integral I_1 can be obtained as

$$I_1 = \sum_{k_0=1}^{K_0+1} \Xi_0(k_0) \sum_{i_0=0}^{\mu_0(k_0)-1} \Lambda_0^{-i_0} \sum_{j_0+l_0=i_0} \frac{e^{-\frac{q_1}{\Lambda_0}}}{(\Lambda_0)^{-\kappa_0}} \Gamma(\kappa_0) \times \frac{(p_0)^{l_0}}{l_0!} \frac{(q_0)^{j_0}}{j_0!} \sum_{k_1=1}^{K_1+1} \Xi_1(k_1) \int_{p_1 x_2 + q_1}^{\infty} x_1^{\kappa_1-1} e^{-\frac{x_1}{\Lambda_1}} dx_1. \quad (78)$$

Further applying [30, Eq. (3.381.3)] and performing some mathematical manipulations, I_1 can be expressed as (36).

In addition, I_2 in (37) can be derived by repeating similar steps when deriving I_0 and I_1 .

APPENDIX B PROOF OF LEMMA 3

The first probability in (41) can be expressed as

$$\begin{aligned} \varrho_1 &= \Pr [g_{\text{CU}}^2 \mathcal{L}_{\text{CU}} > \alpha_1 g_{\text{EU}}^2 \mathcal{L}_{\text{EU}} + a_1, \\ &\quad g_{\text{EU}}^2 \mathcal{L}_{\text{EU}} > \alpha_2 \varphi_{\text{CU}} + a_2, g_{\text{CU}}^2 \mathcal{L}_{\text{CU}} > g_{\text{EU}}^2 \mathcal{L}_{\text{EU}}] \quad (79) \\ &= \Pr [g_{\text{CU}}^2 \mathcal{L}_{\text{CU}} > \alpha_1 g_{\text{EU}}^2 \mathcal{L}_{\text{EU}} + a_1, \\ &\quad g_{\text{EU}}^2 \mathcal{L}_{\text{EU}} > \alpha_2 \varphi_{\text{CU}} + a_2, \alpha_1 g_{\text{EU}}^2 \mathcal{L}_{\text{EU}} + a_1 > g_{\text{EU}}^2 \mathcal{L}_{\text{EU}}] \\ &\quad + \Pr [g_{\text{CU}}^2 \mathcal{L}_{\text{CU}} > h g_{\text{EU}}^2 \mathcal{L}_{\text{EU}}, g_{\text{EU}}^2 \mathcal{L}_{\text{EU}} > \alpha_2 \varphi_{\text{CU}} + a_2, \\ &\quad \alpha_1 g_{\text{EU}}^2 \mathcal{L}_{\text{EU}} + a_1 < g_{\text{EU}}^2 \mathcal{L}_{\text{EU}}]. \quad (80) \end{aligned}$$

where $\varphi_{\text{CU}} \triangleq \left[\tilde{h}_{\text{CU}} \right]^2$. For convenience, let use denote the first and the second probability of (80) as $\varrho_{1,1}$ and $\varrho_{1,2}$, respectively.

A. The probability $\varrho_{1,1}$

For the first probability of (80), considering the case $\alpha_1 < 1$ and $A_1 > a_2$, we have

$$\begin{aligned} \varrho_{1,1} &= \Pr \left[\underbrace{g_{\text{CU}}^2 \mathcal{L}_{\text{CU}} \geq \alpha_1 g_{\text{EU}}^2 \mathcal{L}_{\text{EU}} + a_1}_{X}, A_1 > g_{\text{EU}}^2 \mathcal{L}_{\text{EU}}, \right. \\ &\quad \left. g_{\text{EU}}^2 \mathcal{L}_{\text{EU}} \geq \alpha_2 \varphi_{\text{CU}} + a_2, \mathcal{A} > \varphi_{\text{CU}} \right], \\ &= \Pr [X, g_{\text{EU}}^2 \mathcal{L}_{\text{EU}} > \alpha_2 \varphi_{\text{CU}} + a_2] \\ &\quad - \Pr [X, g_{\text{EU}}^2 \mathcal{L}_{\text{EU}} > \alpha_2 \varphi_{\text{CU}} + a_2, \varphi_{\text{CU}} > \mathcal{A}] \\ &\quad - \Pr [X, g_{\text{EU}}^2 \mathcal{L}_{\text{EU}} > A_1] \\ &\quad + \Pr [X, g_{\text{EU}}^2 \mathcal{L}_{\text{EU}} > A_1, \varphi_{\text{CU}} > \mathcal{A}] \quad (81) \\ &\triangleq \varrho_{1,1}^{(2)} - \varrho_{1,1}^{(1)} - \varrho_{1,1}^{(4)} + \varrho_{1,1}^{(3)}. \quad (82) \end{aligned}$$

By adopting (34), we can derive the ECFEs for $\varrho_{1,1}^{(1)}$, $\varrho_{1,1}^{(2)}$, $\varrho_{1,1}^{(3)}$, and $\varrho_{1,1}^{(4)}$ as

$$\varrho_{1,1}^{(k)} = \sum_{K \geq k \geq 1} \sum_{\substack{\kappa \geq i \geq 0 \\ j+i=i}} \Xi_2([k]_2) J_k, \quad (83)$$

respectively, where $\sum_{K \geq k \geq 1} \equiv \sum_{k_0=1}^{K_0+1} \sum_{k_1=1}^{K_1+1} \sum_{k_2=1}^{K_2+1}$, and $\sum_{\substack{\kappa \geq i \geq 0 \\ j+i=i}} \equiv \sum_{i_0=0}^{\kappa_0-1} \sum_{j_0+l_0=i_0} \sum_{i_1=0}^{\kappa_1-1} \sum_{j_1+l_1=i_1}$.

Considering the case $\alpha_1 \geq 1$, we have

$$\begin{aligned} \varrho_{1,1} &= \Pr [\phi_{\text{CU}} > \alpha_1 \phi_{\text{EU}} + a_1, \phi_{\text{EU}} > \alpha_2 \varphi_{\text{CU}} + a_2] \\ &= \varrho_{1,1}^{(2)} + \begin{cases} \varrho_{1,1}^{(3)} - \varrho_{1,1}^{(1)} - \varrho_{1,1}^{(4)}, & \text{if } \alpha_1 < 1, A_1 > a_2, \\ \varrho_{1,1}^{(2)}, & \text{if } \alpha_1 \geq 1. \end{cases} \quad (84) \end{aligned}$$

B. The probability $\varrho_{1,2}$

For the second probability in (80), we find that $\varrho_{1,2} = 0$ if $\alpha_1 \geq 1$. Considering the case $\alpha_1 < 1$, we have

$$\begin{aligned} \varrho_{1,2} &= \Pr [g_{\text{CU}}^2 \mathcal{L}_{\text{CU}} \geq g_{\text{EU}}^2 \mathcal{L}_{\text{EU}} \geq \alpha_2 \varphi_{\text{CU}} + a_2, g_{\text{EU}}^2 \mathcal{L}_{\text{EU}} > A_1] \\ &= \Pr [g_{\text{CU}}^2 \mathcal{L}_{\text{CU}} \geq g_{\text{EU}}^2 \mathcal{L}_{\text{EU}} \geq \alpha_2 \varphi_{\text{CU}} + a_2, \alpha_2 \varphi_{\text{CU}} + a_2 \geq A_1] \\ &\quad + \Pr [g_{\text{CU}}^2 \mathcal{L}_{\text{CU}} \geq g_{\text{EU}}^2 \mathcal{L}_{\text{EU}} \geq A_1, \alpha_2 \varphi_{\text{CU}} + a_2 < A_1]. \quad (85) \end{aligned}$$

Considering the case $A_1 > a_2$, we have

$$\begin{aligned} \varrho_{1,2} &= \Pr [g_{\text{CU}}^2 \mathcal{L}_{\text{CU}} \geq g_{\text{EU}}^2 \mathcal{L}_{\text{EU}} \geq \alpha_2 \varphi_{\text{CU}} + a_2, \varphi_{\text{CU}} > \mathcal{A}] \\ &\quad + \Pr [g_{\text{CU}}^2 \mathcal{L}_{\text{CU}} \geq g_{\text{EU}}^2 \mathcal{L}_{\text{EU}} \geq A_1, \varphi_{\text{CU}} < \mathcal{A}] \quad (86) \\ &= \Pr [g_{\text{CU}}^2 \mathcal{L}_{\text{CU}} \geq g_{\text{EU}}^2 \mathcal{L}_{\text{EU}} \geq \alpha_2 \varphi_{\text{CU}} + a_2, \varphi_{\text{CU}} > \mathcal{A}] \\ &\quad - \Pr [g_{\text{CU}}^2 \mathcal{L}_{\text{CU}} \geq g_{\text{EU}}^2 \mathcal{L}_{\text{EU}} \geq A_1, \varphi_{\text{CU}} > \mathcal{A}] \\ &\quad + \Pr [g_{\text{CU}}^2 \mathcal{L}_{\text{CU}} \geq g_{\text{EU}}^2 \mathcal{L}_{\text{EU}} \geq A_1], \quad (87) \\ &\triangleq \varrho_{1,2}^{(5)} + \varrho_{1,2}^{(8)} - \varrho_{1,2}^{(7)}, \quad (88) \end{aligned}$$

where $\varrho_{1,2}^{(5)}$, $\varrho_{1,2}^{(8)}$, and $\varrho_{1,2}^{(7)}$ can be obtained by (83).

In addition, for the case $A_1 \leq a_2$, we have

$$\varrho_{1,2} = \Pr [g_{\text{CU}}^2 \mathcal{L}_{\text{CU}} > g_{\text{EU}}^2 \mathcal{L}_{\text{EU}} > \alpha_2 \varphi_{\text{CU}} + a_2] = \varrho_{1,2}^{(6)}. \quad (89)$$

APPENDIX C
PROOF OF LEMMA 4

The second probability in (41) can be expressed as

$$\begin{aligned} \varrho_2 &= \Pr [g_{\text{EU}}^2 \mathcal{L}_{\text{EU}} > \alpha_2 g_{\text{CU}}^2 \mathcal{L}_{\text{CU}} + a_2 g_{\text{EU}}^2 \mathcal{L}_{\text{EU}} < g_{\text{CU}}^2 \mathcal{L}_{\text{CU}}] \\ &= \Pr [g_{\text{EU}}^2 \mathcal{L}_{\text{EU}} > \alpha_2 g_{\text{CU}}^2 \mathcal{L}_{\text{CU}} + a_2, a_2 + \alpha_2 g_{\text{CU}}^2 \mathcal{L}_{\text{CU}} > g_{\text{CU}}^2 \mathcal{L}_{\text{CU}}] \\ &\quad + \Pr [g_{\text{EU}}^2 \mathcal{L}_{\text{EU}} > g_{\text{CU}}^2 \mathcal{L}_{\text{CU}}, a_2 + \alpha_2 g_{\text{CU}}^2 \mathcal{L}_{\text{CU}} < g_{\text{CU}}^2 \mathcal{L}_{\text{CU}}]. \end{aligned} \quad (90)$$

In the case $\alpha_2 < 1$, we can rewrite ϱ_2 as

$$\begin{aligned} \varrho_2 &= \Pr [g_{\text{EU}}^2 \mathcal{L}_{\text{EU}} > \alpha_2 g_{\text{CU}}^2 \mathcal{L}_{\text{CU}} + a_2, g_{\text{CU}}^2 \mathcal{L}_{\text{CU}} > A_1] \\ &\quad - \Pr [g_{\text{EU}}^2 \mathcal{L}_{\text{EU}} > \alpha_2 g_{\text{CU}}^2 \mathcal{L}_{\text{CU}} + a_2] \\ &\quad + \Pr [g_{\text{EU}}^2 \mathcal{L}_{\text{EU}} > g_{\text{CU}}^2 \mathcal{L}_{\text{CU}}, g_{\text{CU}}^2 \mathcal{L}_{\text{CU}} > A_1] \end{aligned} \quad (91)$$

Let us denote the first, the second, and the third probability as $\varrho_2^{(2)}$, $\varrho_2^{(1)}$, and $\varrho_2^{(3)}$, respectively, by adopting (34), we can derive ϱ_2 in the ECFE as

$$\varrho_2 = \varrho_2^{(2)} - \varrho_2^{(1)} + \varrho_2^{(3)}, \quad (92)$$

where

$$\varrho_2^{(k)} = \sum_{k_0=1}^{K_0+1} \sum_{k_1=1}^{K_1+1} \sum_{i_0=0}^{\kappa_0-1} \sum_{j_0+l_0=i_0} \Xi_1(k_1) \hat{J}_k. \quad (93)$$

In the case $\alpha_2 \geq 1$, we have $\varrho_2 = \varrho_2^{(2)}$. Combining the foregoing results, we obtain (44). This completes the proof of Lemma 4.

REFERENCES

- [1] M. Giordani and M. Zorzi, "Non-terrestrial networks in the 6G era: Challenges and opportunities," *IEEE Network*, vol. 35, no. 2, pp. 244–251, Mar. 2021.
- [2] X. Cao, P. Yang, M. Alzenad, X. Xi, D. Wu, and H. Yanikomeroglu, "Airborne communication networks: A survey," *IEEE J. Sel. Areas Commun.*, vol. 36, no. 9, pp. 1907–1926, Sep. 2018.
- [3] D. Wang, M. Giordani, M.-S. Alouini, and M. Zorzi, "The potential of multilayered hierarchical nonterrestrial networks for 6g: A comparative analysis among networking architectures," *IEEE Vehicular Technology Magazine*, vol. 16, no. 3, pp. 99–107, 2021.
- [4] H. Wu, X. Tao, N. Zhang, and X. Shen, "Cooperative UAV cluster-assisted terrestrial cellular networks for ubiquitous coverage," *IEEE J. Sel. Areas Commun.*, vol. 36, no. 9, pp. 2045–2058, Sep. 2018.
- [5] S. Barick and C. Singhal, "Multi-UAV assisted IoT NOMA uplink communication system for disaster scenario," *IEEE Access*, vol. 10, pp. 34 058–34 068, 2022.
- [6] M. Katwe, K. Singh, P. K. Sharma, C.-P. Li, and Z. Ding, "Dynamic user clustering and optimal power allocation in UAV-assisted full-duplex hybrid NOMA system," *IEEE Trans. Wirel. Commun.*, vol. 21, no. 4, pp. 2573–2590, April 2022.
- [7] B. Hu, L. Wang, S. Chen, J. Cui, and L. Chen, "An uplink throughput optimization scheme for UAV-enabled urban emergency communications," *IEEE Internet Things J.*, vol. 9, no. 6, pp. 4291–4302, March 2022.
- [8] B. Clerckx, Y. Mao, R. Schober, E. A. Jorswieck, D. J. Love, J. Yuan, L. Hanzo, G. Y. Li, E. G. Larsson, and G. Caire, "Is NOMA efficient in multi-antenna networks? a critical look at next generation multiple access techniques," *IEEE Open J. Commun. Soc.*, vol. 2, pp. 1310–1343, June 2021.
- [9] Y. Liu, S. Zhang, X. Mu, Z. Ding, R. Schober, N. Al-Dhahir, E. Hossain, and X. Shen, "Evolution of NOMA toward next generation multiple access (NGMA) for 6G," *IEEE Journal on Selected Areas in Communications*, vol. 40, no. 4, pp. 1037–1071, Apr. 2022.
- [10] T.-T. Nguyen, T.-V. Nguyen, T.-H. Vu, D. B. d. Costa, and C. D. Ho, "IoT-based coordinated direct and relay transmission with non-orthogonal multiple access," *IEEE Wirel. Commun. Lett.*, vol. 10, no. 3, pp. 503–507, 2021.
- [11] H. Pan, J. Liang, and S. C. Liew, "Practical NOMA-based coordinated direct and relay transmission," *IEEE Wirel. Commun. Lett.*, vol. 10, no. 1, pp. 170–174, 2021.
- [12] A. Jawarneh, M. Kadoch, and Z. Albatineh, "Decoupling energy efficient approach for hybrid precoding-based mmWave massive MIMO-NOMA with SWIPT," *IEEE Access*, vol. 10, pp. 28 868–28 884, 2022.
- [13] S. Lv, X. Xu, S. Han, X. Tao, and P. Zhang, "Energy-efficient secure short-packet transmission in NOMA-assisted mMTC networks with relaying," *IEEE Trans. Veh. Technol.*, vol. 71, no. 2, pp. 1699–1712, Feb 2022.
- [14] X. Li, Z. Xie, Z. Chu, V. G. Menon, S. Mumtaz, and J. Zhang, "Exploiting benefits of IRS in wireless powered NOMA networks," *IEEE Trans. Green Commun. Netw.*, vol. 6, no. 1, pp. 175–186, March 2022.
- [15] Y. Xu, B. Li, N. Zhao, Y. Chen, G. Wang, Z. Ding, and X. Wang, "Coordinated direct and relay transmission with NOMA and network coding in nakagami- m fading channels," *IEEE Trans. Commun.*, vol. 69, no. 1, pp. 207–222, Jan 2021.
- [16] M. F. Kader, M. B. Shahab, and S. Y. Shin, "Exploiting non-orthogonal multiple access in cooperative relay sharing," *IEEE Commun. Lett.*, vol. 21, no. 5, pp. 1159–1162, 2017.
- [17] Y. Xu, G. Wang, B. Li, and S. Jia, "Performance of D2D aided uplink coordinated direct and relay transmission using NOMA," *IEEE Access*, vol. 7, pp. 151 090–151 102, Oct. 2019.
- [18] Y. Xu, J. Cheng, G. Wang, and V. C. M. Leung, "Adaptive coordinated direct and relay transmission for NOMA networks: A joint downlink-uplink scheme," *IEEE Trans. Wirel. Commun.*, vol. 20, no. 7, pp. 4328–4346, July 2021.
- [19] M. F. Kader and S. Y. Shin, "Coordinated direct and relay transmission using uplink NOMA," *IEEE Wirel. Commun. Lett.*, vol. 7, no. 3, pp. 400–403, June 2018.
- [20] Y. Liu, M. Derakhshani, and S. Lambotharan, "Outage analysis and power allocation in uplink non-orthogonal multiple access systems," *IEEE Commun. Lett.*, vol. 22, no. 2, pp. 336–339, Feb 2018.
- [21] A. Agarwal, R. Chaurasiya, S. Rai, and A. K. Jagannatham, "Outage probability analysis for NOMA downlink and uplink communication systems with generalized fading channels," *IEEE Access*, vol. 8, pp. 220 461–220 481, Dec. 2020.
- [22] M.-T. Nguyen, T.-H. Vu, and S. Kim, "Performance analysis of wireless powered cooperative NOMA-based CDRT IoT networks," *IEEE Syst. J.*, pp. 1–12, 2022.
- [23] P. K. Sharma and D. I. Kim, "Coverage probability of 3-D mobile UAV networks," *IEEE Wirel. Commun. Lett.*, vol. 8, no. 1, pp. 97–100, Feb 2019.
- [24] R. Amer, W. Saad, and N. Marchetti, "Mobility in the sky: Performance and mobility analysis for cellular-connected UAVs," *IEEE Trans. Commun.*, vol. 68, no. 5, pp. 3229–3246, May 2020.
- [25] Y. Gao, B. Xia, K. Xiao, Z. Chen, X. Li, and S. Zhang, "Theoretical analysis of the dynamic decode ordering SIC receiver for uplink NOMA systems," *IEEE Commun. Lett.*, vol. 21, no. 10, pp. 2246–2249, June 2017.
- [26] Y. Gao, B. Xia, Y. Liu, Y. Yao, K. Xiao, and G. Lu, "Analysis of the dynamic ordered decoding for uplink NOMA systems with imperfect CSI," *IEEE Trans. Veh. Technol.*, vol. 67, no. 7, pp. 6647–6651, July 2018.
- [27] A. Zakeri, M. Moltafet, and N. Mokari, "Joint radio resource allocation and SIC ordering in NOMA-based networks using submodularity and matching theory," *IEEE Trans. Veh. Technol.*, vol. 68, no. 10, pp. 9761–9773, Oct. 2019.
- [28] I. S. Gradshteyn and I. M. Ryzhik, *Tables of Integrals, Series, and Products*, 7th ed. New York, NY, USA: Academic Press, 2007.
- [29] Y. J. Chun, S. L. Cotton, H. S. Dhillon, F. J. Lopez-Martinez, J. F. Paris, and S. K. Yoo, "A comprehensive analysis of 5g heterogeneous cellular systems operating over $\kappa - \mu$ shadowed fading channels," *IEEE Trans. Wirel. Commun.*, vol. 16, no. 11, pp. 6995–7010, Aug. 2017.
- [30] A. Jeffrey and D. Zwillinger, *Table of integrals, series, and products*. Academic press, 2007.
- [31] G. T. RP-150496, "Study on Downlink Multiuser Superposition Transmission."
- [32] A. Al-Hourani, S. Kandeepan, and S. Lardner, "Optimal LAP altitude for maximum coverage," *IEEE Wirel. Commun. Lett.*, vol. 3, no. 6, pp. 569–572, July 2014.
- [33] L. Yuan, N. Yang, F. Fang, and Z. Ding, "Performance analysis of UAV-assisted short-packet cooperative communications," *IEEE Trans. Veh. Technol.*, pp. 1–1, Jan. 2022.
- [34] W. Mei and R. Zhang, "Uplink cooperative NOMA for cellular-connected UAV," *IEEE Journal of Selected Topics in Signal Processing*, vol. 13, no. 3, pp. 644–656, 2019.
- [35] S. Atapattu, C. Tellambura, and H. Jiang, "A mixture Gamma distribution to model the SNR of wireless channels," *IEEE Trans. Wirel. Commun.*, vol. 10, no. 12, pp. 4193–4203, December 2011.